

Vertical distribution of microphysical properties of Arctic springtime low-level mixed-phase clouds over the Greenland and Norwegian Seas

Guillaume Mioche^{1,2}, Olivier Jourdan^{1,2}, Julien Delanoë³, Christophe Gourbeyre^{1,2}, Guy Febvre^{1,2}, Régis Dupuy^{1,2}, Marie Monier^{1,2}, Frédéric Szczap^{1,2}, Alfons Schwarzenboeck^{1,2}, and Jean-François Gayet^{1,2}.

¹ Université Clermont Auvergne, OPGC, Laboratoire de Météorologie Physique, F-63000 Clermont-Ferrand, France

² CNRS, UMR 6016, LaMP/OPGC, BP80026, 63177 Aubière, France

³ Laboratoire Atmosphère, Milieux et Observations Spatiales, UVSQ/CNRS/UPMC-IPSL, 78035, Guyancourt, France

Correspondence to: Guillaume Mioche (g.mioche@opgc.fr) and Olivier Jourdan (o.jourdan@opgc.fr)

Abstract. This study aims to characterize the microphysical and optical properties of ice crystals and supercooled liquid droplets within low-level Arctic mixed-phase clouds (MPCs). We compiled and analyzed cloud *in situ* measurements from 4 airborne spring campaigns (representing 18 flights and 71 vertical profiles in MPCs) over the Greenland and Norwegian Seas mainly in the vicinity of the Svalbard Archipelago. Cloud phase discrimination and representative vertical profiles of number, size, mass and shape of ice crystals and liquid droplets are established. The results show that the liquid phase dominates the upper part of the MPCs. High concentrations (120 cm^{-3} in average) of small droplets (mean values of $15 \text{ }\mu\text{m}$), with an averaged LWC of $0.2 \text{ g}\cdot\text{m}^{-3}$ are measured at cloud top. The ice phase dominates the microphysical properties in the lower part of the cloud and beneath it, in the precipitation region (mean values of $100 \text{ }\mu\text{m}$, 3 L^{-1} and $0.025 \text{ g}\cdot\text{m}^{-3}$ for diameter, particle concentration and IWC respectively). The analysis of the ice crystal morphology shows that the majority of ice particles are irregularly shaped or rimed particles, the prevailing regular habits found are stellars and plates. We hypothesize that riming and diffusional growth processes (including the Wegener-Bergeron-Findeisen mechanism) are the main growth mechanisms involved in the observed MPCs. The impact of larger scale meteorological conditions on the vertical profiles of MPC properties was also investigated. Large values of LWC and high concentration of smaller droplets are possibly linked to polluted situations and air masses origins from the South, which lead to very low values of ice crystal size and IWC. On the contrary, clean situations with low temperatures exhibit larger values of ice crystal size and IWC. Several parameterizations relevant for remote sensing or modeling studies are also determined, such as IWC (and LWC) – extinction relationship, ice and liquid integrated water paths, ice concentration and liquid water fraction according to temperature.

1. Introduction

The Arctic region is more sensitive to climate change than any other region of the Earth (Solomon et al., 2007). Clouds and particularly low-level mixed-phase clouds related processes have a major impact on the Arctic

39 surface energy budget (**Curry, 1995; Curry et al., 1996; Morrison et al., 2011**). Observations suggest that
40 boundary layer mixed phase clouds (MPCs, mixture of liquid droplets and ice) are ubiquitous in the Arctic and
41 persist for several days under a variety of meteorological conditions (**Mioche et al., 2015; Morrison et al.,
42 2012; Shupe et al., 2011; Shupe and Intrieri, 2004**). They occur as single or multiple stratiform layers of
43 supercooled droplets near the cloud top in which ice crystals can form and precipitate. These clouds have a large
44 impact on the surface radiative fluxes and Arctic climate feedbacks (**Kay et al., 2012; Kay and Gettelman,
45 2009**). The strong impact of MPCs on the energy budget stems from their persistence and microphysical
46 properties which result from a complex web of interactions between numerous local and larger scale processes
47 that greatly complicate their understanding and modeling (**Klein et al., 2009; Morrison et al., 2012**).

48 However, major uncertainties limit our understanding of the interactions and feedbacks between the physical
49 processes involved in their life cycle. This complexity translates in the large discrepancies that can be found in
50 numerical models to represent the cloud processes, which in turn impacts their capability to forecast cloud
51 properties in the Arctic. For instance, Global Climate Models (GCM) tend to underestimate the amount of liquid
52 water in MPCs (**Komurcu et al., 2014**). Therefore, the representation of ice formation and growth processes and
53 their interactions with the liquid phase (e.g. liquid/ice partitioning, Wegener-Bergeron-Findeisen process) has to
54 be improved, as already shown in previous modelling studies (**Prenni et al. (2007)** or **Klein et al. (2009)**).

55 Among the various cloud properties which need to be described more accurately, the cloud thermodynamic
56 phase is a parameter of primary importance since it governs the cloud optical and therefore radiative properties
57 as well as its life cycle (longevity and precipitation formation).

58 However, measuring the spatial phase distribution in low level arctic mixed-phase clouds, in order to relate it to
59 environmental conditions (height, temperature, surface conditions, air mass origins...) to parameterize and
60 model it, remains a challenge. The parameterizations of liquid and ice partitioning in numerical simulations vary
61 from one model to another. A study carried out by **Klein et al. (2009)** compared outputs from 26 different
62 numerical models. They found that using different schemes of temperature dependent partitioning yield to liquid
63 water content ranging from 12 % to 83 % for a same cloud top temperature of -15°C.

64 Beyond the experimental limitations related to the accurate measurement of the phase partitioning (discussed
65 hereafter), the cloud phase quantification is also hampered by difficulties to translate observational
66 characterization into realistic representations for cloud models with a wide range of scales. The definition of
67 mixed phase system is actually controversial. A mixed phase cloud can be regarded as a complete cloud system
68 that contains both liquid and ice involved in mixed microphysical processes but does not necessarily implies that
69 all volumes in the system contain both phases (**Shupe et al., 2008**). Additionally, the definition of a mixed phase
70 cloud or volume could be based either on a threshold value for its optical properties or for the ratio between
71 supercooled liquid droplets and ice crystal mass or number (**Cober et al., 2001**). The threshold values are
72 questionable. The standard assumption in climate models is that liquid and ice are uniformly mixed throughout
73 each entire model grid box (with a typical horizontal resolution of 100 km and 1 km in the vertical, **Tan and
74 Storelvmo (2016)**). However some field measurements (see among others **Rangno and Hobbs (2001)** or
75 **Korolev and Isaac (2003)**) suggest that different pockets of solely water or ice in mixed phase regions coexist
76 with typical scale of tens of meters. This has consequences on how processes like the Wegener-Bergeron-
77 Findeisen process should be parameterized in large scale models.

78

79

80 A better assessment of the ice/liquid partitioning will improve our understanding of the life cycle and more
81 precisely the persistence of MPCs since modelling studies show that this persistence is governed by a delicate
82 balance between dynamical, radiative and microphysical processes occurring mainly in the boundary layer
83 (**Savre and Ekman, 2015**). This understanding is still limited by the description of the microphysical processes
84 related to the initiation and the maintenance of the ice phase. The cloud processes responsible for the production
85 of ice crystals in the upper part of the cloud seems to be mostly driven by the cloud top temperature and the
86 entrainment rates (**Savre and Ekman, 2015**). In particular, the assessment of IN concentration and its time
87 evolution is of primary importance rely on a very limited set of *in situ* observations and need to be improved
88 (**Ovchinnikov et al., 2014**). The ice crystal number concentrations usually exceed the number of IN particles.
89 These discrepancies could be explained by the limitations of *in situ* instruments and especially the
90 overestimation of the ice crystal number due to the shattering of large ice crystals on the probe inlets or the
91 inability of instrument measuring IN particles to detect all the activation modes (**Baumgardner et al., 2012**;
92 **Korolev et al., 2011**). Secondary ice formation processes or the recycling of IN particles through subcloud
93 sublimation (**Lawson et al., 2001**; **Rangno and Hobbs, 2001**; **Solomon et al., 2015**) may also play an important
94 role and explain such discrepancies. Given the temperatures observed in MPCs, heterogeneous ice nucleation
95 mechanisms are preferentially involved. The concentration of large ice crystals ($> 100 \mu\text{m}$) in particular may be
96 due to heterogeneous ice formation mechanisms (**Eidhammer et al., 2010**; **Prenni et al., 2009**). However which
97 process, among deposition, condensation, immersion or contact freezing processes, is mainly responsible for the
98 initiation of ice crystals is still under debate as modeling studies fail to reproduce the observed ice number
99 concentration (**Avramov and Harrington, 2010**; **Fridlind et al., 2007**). In a recent modeling study linked to the
100 Aerosol-Cloud Coupling and Climate Interactions in the Arctic (ACCACIA) campaign, **Young et al. (2017)**
101 showed that small differences in the predicted ice concentration can have large effects on the microphysical
102 structure (such as ice/liquid partitioning) and life time of single layer MPCs. They suggested that the method of
103 parameterizing primary ice concentration in bulk microphysical models is therefore of primary importance.

104

105 The recent developments of ground based stations (Barrow, EUREKA, NY-Alesund among others) and
106 spaceborne remote sensing observations (as lidar and radar observations from the CALIPSO and CloudSat
107 platforms respectively) allow today reliable studies of Arctic cloud phase variability from a few km to the pan-
108 arctic region (**Dong et al., 2010**; **Kay and Gettelman, 2009**; **Liu et al., 2012**; **Shupe et al., 2011**). Moreover,
109 remote sensing observations from space performed by active instruments onboard CALIPSO (**Winker et al.,**
110 **2003**) and CloudSat (**Stephens et al., 2002**) satellites as a part of the A-Train constellation provide a unique way
111 of characterizing Arctic cloud vertical properties. However, the cloud phase distribution and characterization are
112 highly dependent of the measurement principle of the instruments.

113 The aforementioned techniques provide cloud properties typically averaged over one kilometer, which may be
114 insufficient to study cloud processes at a microphysical scale (i.e. measurements of microphysical cloud
115 properties, spatial resolution less or equal to 100 m). *In situ* observations are based on direct measurement
116 techniques at a higher spatial resolution (generally < 100 m). Numerous previous studies dedicated to the
117 assessment of the *in situ* microphysical properties of Arctic clouds focused on specific case studies (**Avramov et**
118 **al., 2011**; **Gayet et al., 2009**; **Rangno and Hobbs, 2001**; **Verlinde et al., 2007**). Statistical analysis of mixed

119 phase cloud properties derived from several *in situ* datasets or airborne campaigns are very scarce and often
120 focus on the Western Arctic region (McFarquhar et al., 2007; Jackson et al., 2012). Such data analysis
121 strategy is still missing in the European Arctic Region (and in the vicinity of Svalbard, over the Greenland and
122 Norwegian Seas in particular).

123 In Mioche et al. (2015), the spatial, seasonal, and surface conditions variability of MPC properties using
124 CloudSat and CALIPSO spaceborne observations has been investigated. The study showed a large occurrence of
125 MPCs all year long both over the whole Arctic and the Svalbard regions. It was clearly evidenced that the
126 Svalbard region, due to its specific location near the Atlantic Ocean, presents a larger occurrence of low level
127 MPCs compared to the averaged Arctic. Then, it appears important to investigate the microphysical properties of
128 MPCs in the Svalbard / Greenland Sea regions from a statistical point of view to provide representative profiles
129 that can be compared to previous works focused on the Western Arctic region.

130
131 This work provides statistics analysis of liquid and ice properties of low level Arctic MPCs from *in situ* data
132 collected in single layer MPCs during several airborne campaigns in the region of Norwegian/Greenland Sea
133 carried out between 2004 and 2010. We compiled observations of microphysical composition of Arctic mixed
134 phase clouds (cloud phase, hydrometeors number, mass and shape) to present vertical profiles of liquid and ice
135 properties. The main objective is a step to a better understanding of the processes involved in Arctic low-level
136 MPC life cycle at the microphysical scale. We aimed to relate these properties to environmental conditions in
137 order to improve the cloud parameterizations used in models and remote sensing algorithms. The results will
138 also complement previous works concerning Arctic clouds characterizations performed in Western Arctic.

139
140 This paper is organized in four sections. The description of the field experiments, instrumentation and datasets
141 will be made in section 2. Section 3 will present and discuss the vertical profiles of microphysical properties of
142 the low-level MPCs. Finally, key parameterizations useful for modeling or remote sensing will be proposed in
143 section 4.

144

145 2 Field experiments, airborne measurements and meteorological situations

146

147 2.1 Airborne campaigns

148 This study is based on *in situ* data collected in single-layer mixed-phase clouds (MPCs) during four international
149 airborne campaigns organized in the “European” Arctic region, namely:

150 (i) and (ii) the Arctic Study of Tropospheric Aerosols, clouds and Radiation experiments (ASTAR, Herber et
151 al., 2004; Jourdan et al., 2010; Ehrlich et al., 2009; Gayet et al., 2009; Lampert et al., 2009) which took
152 place in the vicinity of Svalbard (Longyearbyen, Norway, 78° N, 15° E) in April 2004 and April 2007. The
153 Polar-2 aircraft operated by AWI (Alfred Wegener Institute) was flown during these two experiments;

154 (iii) the Polar Study using Aircraft, Remote Sensing, Surface Measurements and Models, of Climate, Chemistry,
155 Aerosols, and Transport (POLARCAT-France, Delanoë et al., 2013; Law et al., 2008; Quennehen et al., 2011)
156 which was carried out in northern Sweden (Kiruna, 68° N, 20° E) in April 2008 during the International Polar
157 Year. Measurements were performed onboard the French ATR-42 aircraft of SAFIRE (Service des Avions
158 Français Instrumentés pour la Recherche en Environnement);

159 and (iv) the Solar Radiation and Phase Discrimination of Arctic Clouds experiment (SORPIC, **Bierwirth et al.,**
160 **2013**), in the Svalbard region in May 2010 with the AWI Polar-5 aircraft.

161 All the clouds sampled during these four campaigns were located over the Arctic Greenland and Norwegian seas
162 as displayed on Fig. 1. The scientific flights during ASTAR and SORPIC covered latitudes ranging from 75° N
163 to 79° N (Greenland Sea) while the flights during POLARCAT were performed between 70° N and 73° N
164 (Norwegian Sea). Moreover, the data were all collected during spring (April and May).

165 For this study, we restricted the measurements to continuous ascent and descent flight sequences into single-
166 layer MPCs at the aircraft speed (between 80m/s and 100 m/s for all campaigns) since our main objective is to
167 study the vertical partitioning of ice and liquid thermodynamical phases. Our dataset consists of 71 cloud
168 profiles (see Table 1) representing more than 21 000 measurement points at 1Hz (350 minutes of cloud
169 observations), spread out over 18 flights performed above arctic open sea water.

170

171 **2.2 *In situ* instrumentation**

172

173 A similar *in situ* instrumentation was loaded on the three aircraft: the German Polar-2 and Polar-5 and the French
174 ATR-42. The same data processing procedure was used in order to derive the cloud microphysical parameters (at
175 a same scale: i.e. ~ 100 m). This consistent cloud data set is used to achieve a statistically representative
176 description of the properties of Arctic mixed-phase clouds sampled over the Greenland and Norwegian Seas
177 during spring.

178 The suite of *in situ* instruments used to measure the MPC microphysical and optical properties consists of:

- 179 - the Cloud Particle Imager (CPI, **Lawson et al., 2001**), which captures cloud particle images on a
180 1024x1024 pixels CCD camera with a pixel resolution of 2.3 μm and with 256 grey levels. At least 5
181 pixels are necessary to identify a cloud particle, so the particle sizes derived from the CPI range from 15
182 μm to approximately 2 mm. The images are processed using the software developed at the Laboratoire
183 de Météorologie Physique (LaMP, **Lefèvre, 2007**) based on the original CPIView software (CPIView,
184 2005, **Lawson et al., 2001; Baker and Lawson, 2006**). In particular, it provides particle size
185 distribution (PSD) and derived microphysical parameters such as particle concentration, effective
186 diameter, extinction coefficient and ice water content as well as a particle habit classification. The data
187 processing method used to derive the extinction coefficient (σ) and the Ice Water Content (IWC) is
188 described in Appendix A;
- 189 - the PMS Forward Scattering Spectrometer Probe (FSSP-100, **Baumgardner et al., 2002; Knollenberg,**
190 **1981**); it provides the droplet size distribution from 3 to 45 μm . The derived parameters from the PSD
191 are the droplet concentration, the effective diameter, the extinction coefficient (σ) and the liquid water
192 content (LWC);
- 193 - the Polar Nephelometer (PN, **Gayet et al., 1997**) which measures the angular scattering intensities (non
194 normalized scattering phase function) of an ensemble of cloud particles (either droplets, ice crystals or a
195 mix), from a few micrometers to about 800 μm . In particular, these measurements are used to identify
196 spherical from non-spherical particles and thus discriminate the dominant cloud thermodynamical

197 phase. The extinction coefficient and the asymmetry parameter (g) are calculated following the
198 methodology presented in **Gerber et al. (2000)** and **Gayet et al. (2002)**;
199 - the Nevzorov probe (**Korolev et al., 1998**), which uses the hot-wire technique to retrieve the liquid
200 water content and the total water content. Note that the Nevzorov data are only used to determine liquid
201 water content during ASTAR 2004 because the FSSP-100 was not used during this campaign. The
202 retrieval method used to determine the liquid water content is described in Appendix A.

203
204 All these cloud probes were heated in order to avoid icing during the flights. The combination of these probes
205 provides the microphysical properties of cloud particles from a few micrometers (typically 3 μm) to about 2 mm.
206 Data are recorded at 1 Hz frequency which corresponds to a spatial resolution of about 100 m (according to the
207 aircraft speed). The uncertainties and measurement ranges associated to the derived cloud parameters are
208 summarized in Table 2. However it should be noted that *in situ* measurements accuracy may be hampered by the
209 shattering of large ice crystals on the probe inlets, inducing smaller particle artifact (**Heymsfield, 2007**) leading
210 to an overestimation of small particle concentration. For example, previous studies of **Field et al. (2003)** and
211 **Heymsfield (2007)** showed that shattering effect may lead to an overestimation of about 20 % on the bulk
212 properties and a factor 2 or 3 on the number concentration of ice crystals. Moreover, the recent study by **Guyot**
213 **et al. (2015)** that compared on *in situ* measurements with the same probes and similar inlet design in a wind
214 tunnel experiment showed that measured particles can vary from one instrument to another and careful
215 calibration is needed. Even though no standard method was available during the campaigns to accurately
216 determine and remove the impact of shattering (designed tips, particle interarrival time measurement...), a short
217 analysis is described in Appendix B for the control of the data quality and the significance of shattering effect.
218 Comparing the extinction coefficient measured by the PN measurements to the extinction derived from the
219 combination of the CPI and FSSP measurements showed that the shattering effect, in our case, was smaller than
220 the measurements uncertainties (i.e. 25 %, 35 % and 55 % for PN, FSSP and CPI respectively see Table 2).

221 The three research aircraft also measured basic meteorological parameters along the flight track (see
222 **Gayet et al., 2009**). We recall that the static air temperature is calculated with an accuracy better than ± 0.5 K. If
223 high liquid water contents can alter these temperature measurements, the observed contents, lower than $0.6 \text{ g}\cdot\text{m}^{-3}$
224 during most of the MPC flights, ensure that this effect was not significant along the cloud transects. The altitude
225 and geographical position parameters were measured by the airborne GPS systems with an accuracy of 50 m.

227 2.3. Normalized altitudes

228
229 Table 3 summarizes, for the 71 selected profiles, the statistics of altitudes for MPCs top and base, as well as the
230 thickness of the cloud layer containing liquid water. The mean cloud top altitude is located around 1200 ± 310 m
231 while the mean cloud base altitude (referring as the altitude below which liquid phase is no longer present) is 756
232 ± 283 m. This is consistent with observations performed in western Arctic where cloud top altitudes lie between
233 885 m and 1320 m, and cloud base altitudes between 420 m and 745 m (**McFarquhar et al., 2007**). Our
234 measurements also indicate that the thickness of the liquid layer spans from 100 m to 950 m with an averaged
235 value of 444 m. The objective of this study is to merge and analyze the MPC microphysical data obtained during
236 the four airborne campaigns to derive representative vertical profiles. Since cloud top and cloud base heights

237 exhibit large variability (see Table 3), the altitudes are normalized following the method presented in **Jackson et**
 238 **al. (2012)**. The cloud top and cloud base refer to the liquid phase layer, i.e. the cloud layers containing liquid
 239 droplets (mixed phase or liquid only). These layers are identified based on the PN asymmetry parameter values
 240 greater than 0.8 (**Jourdan et al. (2010)**, see section 2.4. below). Within these layers (Eq. (1)) and below the
 241 cloud base (Eq. (2)) the normalized altitudes Z_n are defined as follow:

$$242 \quad Z_n = \frac{z - z_b}{z_t - z_b} \quad \text{for } z_b < z < z_t \quad (1)$$

$$243 \quad Z_n = \frac{z}{z_b} - 1 \quad \text{for } z < z_b \quad (2)$$

244
 245 where Z_n is the normalized altitude, Z the altitude corresponding to the aircraft measurements, Z_t and Z_b the
 246 cloud top and base altitudes respectively. Thus, an altitude of 1 corresponds to the top of the cloud liquid
 247 containing layer and 0 to its base. Negative values characterize regions of ice precipitation below the cloud layer
 248 and the altitude of -1 defines the ground level according to Eq. (2).

249 To obtain representative statistical results, the cloud layers have been stratified in 10 levels with intervals of 0.2
 250 of normalized altitude, each containing around 2000 observations (i.e. about 10% of the data set). The vertical
 251 profiles of MPC microphysical properties presented hereafter are obtained by averaging the *in situ* measurements
 252 over each normalized altitude layer. The profiles are computed for the whole data set and for each main
 253 meteorology situation separately (see section 2.5) for a better analysis and discussions of the results.

254 **2.4. Determination of the cloud thermodynamical phase from *in situ* measurements**

255
 256 As stated above, the asymmetry parameter (g) derived from the PN scattering phase function (PhF)
 257 measurements is used to discriminate cloud thermodynamic phase. Indeed, in a previous study, **Jourdan et al.**
 258 **(2010)** have shown with a principal component analysis that g is a reliable proxy to determine the cloud phase of
 259 Arctic MPCs. One can notice that our phase discrimination is considered from an optical point of view and
 260 differs from the one used by **Korolev et al. (2003)** which is based on the ice water fraction (IWC/TWC) to
 261 identify cloud phase. Large values of g (> 0.83) are typical of an ensemble of particles optically dominated by
 262 liquid water droplets where ice crystals do not significantly affect the optical properties. On the contrary, smaller
 263 values of g (< 0.80) are characteristic of a cloud optically dominated by ice crystals, with negligible contribution
 264 of liquid droplets. For g ranging from 0.80 to 0.83, both liquid droplets and ice crystals contribute to the optical
 265 properties. The optical signature of the ice is more pronounced (i.e. g decreases) as the concentration and/or the
 266 size of ice particles becomes larger. These results are well illustrated and discussed by **Febvre et al. (2012)**
 267 where PN measurements were combined with FSSP and CPI data.

268 Figure 2 displays the mean PN scattering phase function (Fig. 2a) according to the normalized MPC altitude
 269 levels as well as the vertical profile of the corresponding g -values (Fig. 2b). At cloud top, the PhF is
 270 characterized by a rather high scattering at forward angles (angles lower than 60°) associated to lower scattering
 271 at sideward angles (60 - 130°), and enhanced scattering around 140° . These features are representative of cloud
 272 layers dominated by spherical particles (mainly supercooled liquid droplets), corresponding to typical g -values
 273 greater than 0.83. As Z_n decreases, the PhF becomes smoother and more featureless. A side scattering
 274

277 enhancement is observed along with an attenuation of the 140° peak. This behavior can be attributed to the
278 presence of non-spherical ice crystals increasing towards the cloud base. This is in agreement with the
279 continuous decrease of g-values observed from cloud top (0.84) to cloud base (0.82). Figure 2 also shows that
280 the ice phase region below the cloud layer ($-1 < Z_n < 0$) is characterized by a featureless and flat (at side
281 scattering angles) PhF, with no significant influence of the altitude. These PhF are associated to g-values smaller
282 than 0.8. It is thus clearly shown that the PhF and asymmetry parameter are related to specific microphysical
283 properties encountered at different cloud levels. These observations demonstrate that the PhF and the asymmetry
284 parameter can be regarded as an accurate signature of the main microphysical properties observed in the MPC
285 layers particles.

286 The liquid droplets properties are determined from the FSSP or Nevzorov probe measurements when g-values
287 are greater than 0.8 (i.e. indicating a “liquid-containing” phase). Accordingly, the ice crystals properties are
288 derived from CPI measurements when g-values are lower than 0.83 (i.e. indicating an “ice-containing” phase).
289 For g ranging between 0.8 and 0.83, both liquid and ice properties are derived. Moreover, CPI particle images
290 classified as spherical droplets are not taken into account for the determination of ice crystal microphysical
291 parameters. Table 4 summarizes the cloud phase analysis.

292
293

294 2.5. Meteorological situations

295

296 All the selected situations correspond to low-level single layer mixed-phase clouds in the boundary layer during
297 spring. If these criteria ensure the homogeneity of the dataset, weather conditions still vary significantly from
298 one campaign to another or even within a campaign. In order to provide a comprehensive dataset to improve
299 model parameterization, this is of great importance to discriminate and classify the observations depending on
300 environmental conditions. The most trivial classification is the temperature regime. **Savre and Ekman (2015)**,
301 showed that it is one of the major factors (with cloud top entrainment) controlling the production of new ice
302 crystals and the maintenance of MPCs. In the present study, two temperature regimes have been selected based
303 on the mean cloud top temperature of each situation: the “cold” situations ($-22\text{ °C} < T_{\text{Top}} < -15\text{ °C}$) and the
304 “warm” situations ($-15\text{ °C} < T_{\text{Top}} < -8\text{ °C}$). In spring, the cold polar vortex that covers the Arctic Region weakens
305 and inclusions of midlatitude air masses are more likely. Atmospheric properties such as temperature, humidity,
306 and particles loading can change significantly. Arctic cloud properties are then strongly linked to the air mass
307 origin (**Gultepe et al., 2000; Gultepe and Isaac, 2002**), since their formation is driven by the aerosol particles
308 properties and thermodynamical and dynamical conditions. For these reasons, we also included the air mass
309 origin in the classification, which was determined from the analysis of back-trajectories computed with the
310 NOAA HySPLIT model (Hybrid Single-Particle Lagrangian Integrated Trajectory model, **Draxler and Rolph,**
311 **2003**). The backtrajectories can be classified in two kinds: the air masses originating from the North (over sea ice
312 or open water of the Arctic Ocean and Greenland Sea) that are cold and clean, and the air masses more
313 continental which have travelled over more polluted regions in the South and/or East. We made the choice of
314 only two temperature regimes and two main air mass origin in order to ensure representative and statistically
315 significant datasets for each class. Table 5 shows that all the cold situations are correlated with a north origin air
316 mass (blue in Table 5). Among the 12 warm situations, 7 correspond to air masses originating from North (green

317 in Table 5) and 5 from South/East (red in Table 5). So, at the end, this classification leads to only 3 types of
318 situations: (i) Cold cloud top temperature situations with air masses originating always from the North (hereafter
319 referred as COLD in the manuscript); Warmer situations with air masses which has its origin either (ii) in the
320 North (hereafter WARM_NO cases) or (iii) from the continent: South and East (hereafter WARM_SO cases).
321 The mean vertical profiles of temperature of these 3 regimes are displayed on Fig. 3. The results show a well
322 pronounced temperature inversion (~ -10 °C) for the WARM_SO situations whereas WARM_NO cases do not
323 exhibit such clear temperature inversion. The COLD situations are characterized by a temperature of -20 °C at
324 cloud top and by weather situations dominated by cold air outbreaks from higher latitudes (Gayet et al., 2009).
325

326 3. Vertical properties of liquid droplets and ice crystal particles within MPCs

327
328 The purpose of this section is to provide a quantitative assessment of the average microphysical and optical
329 properties of the MPC cloud layers at a spatial scale of approximately 100 m. The vertical profiles presented in
330 this study come from aircraft *in situ* measurements and are obtained from several distinctive clouds. It should be
331 emphasized that these profiles cannot be strictly regarded as vertical and instantaneous profiles (each ascending
332 or descending flight sequence is generally made in 5 to 10 minutes). It differs from the remote sensing
333 measurements that usually provide snapshots of a same cloud.
334

335 3.1. Liquid phase properties

336
337 Figure 4 displays the average vertical profiles expressed with the normalized altitude reference for the liquid
338 phase properties: the extinction coefficient, the droplet number concentration, the liquid water content and the
339 effective diameter (Figs. 4a to 4d). These profiles are obtained using FSSP-100 or Nevzorov probe
340 measurements and constrained by PN g-values greater than 0.8. On this figure, the average profiles for liquid
341 properties are discriminated for each environmental conditions class: COLD in blue, WARM_NO in green and
342 WARM_SO in red. The mean profile corresponding to the average over all situations (or campaigns) is also
343 shown (in black). The average vertical distribution for the liquid droplet number size distribution is shown in
344 Fig. 4e.

345 The MPC properties are characterized by increasing values of LWC with altitude. LWC mean values range
346 between 0.1 g.m^{-3} at the bottom of the liquid layer and nearly 0.2 g.m^{-3} close to the cloud top. The concentration
347 of cloud droplets remains nearly constant throughout the MPC layers with mean values around 120 cm^{-3} .
348 However smaller values are observed near the cloud top. Clouds corresponding to the WARM_SO situations are
349 characterized by larger values of droplet concentration and LWC (200 cm^{-3} and 0.3 g.m^{-3}) compared to the
350 COLD and WARM_NO cases. . This is related to the fact that air masses originating from midlatitudes are more
351 humid. The extinction coefficient profiles are correlated with the LWC measurements indicating that liquid
352 droplets mainly drive the optical properties of the upper MPC layers. This is consistent with the observed shape
353 of the scattering phase function at cloud top displayed in Figure 2. The extinction coefficient presents maximum
354 values in the upper part of the cloud (average around 25 km^{-1}), and smaller extinction in the lower part of the
355 liquid layer (down to 15 km^{-1}). Finally, the vertical profiles of the effective diameter (Fig. 4a) and droplet
356 number size distribution (Fig. 4e) are consistent with the extinction coefficient, LWC and droplet concentration.

357 Indeed, the effective diameter is proportional to the ratio of the LWC to the extinction coefficient. The cloud
358 layers dominated by the liquid phase exhibit small droplet sizes, with a slight increase of the diameter from cloud
359 base to cloud top (from 10 to 15 μm).

360 The main features of the vertical distribution for the liquid phase properties are in agreement with previous
361 observations (e.g. **Lawson et al. (2001)**, **McFarquhar et al. (2007)** or **Jackson et al. (2012)**). These studies
362 focused on MPCs in the western arctic region under meteorological situations that can be connected to the ones
363 presented in our work. **Lawson et al. (2001)** studied a boundary layer MPC in spring over the Beaufort Sea
364 during the First International Satellite Cloud Climatology Regional Experiment Arctic Cloud Experiment (FIRE-
365 ACE). The temperature range lied between $-22\text{ }^{\circ}\text{C}$ and $-25\text{ }^{\circ}\text{C}$. This case could be regarded as the COLD
366 situations in our study. **Lawson et al. (2001)** showed LWC values around $0.15\text{ g}\cdot\text{m}^{-3}$ and droplet concentration
367 close to 200 cm^{-3} .

368 **McFarquhar et al. (2007)** merged 4 MPC situations (corresponding to 53 cloud profiles) in autumn over
369 Barrow and Oliktok Point, Alaska during the Mixed-Phase Arctic Cloud Experiment (M-PACE). The MPCs
370 were associated with a low-level northeasterly flow over the ice pack resulting in persistent roll clouds at low-
371 level altitude. Cloud top temperatures lied between $-12\text{ }^{\circ}\text{C}$ and $-16\text{ }^{\circ}\text{C}$. These situations can be related to our
372 COLD and WARM_NO cases. They also observed the increase of liquid droplet size, LWC and number
373 concentration with the altitude. The LWC range ($0.15\text{-}0.19\text{ g}\cdot\text{m}^{-3}$) is consistent with our study but the droplet size
374 range (from $14\mu\text{m}$ at cloud base to $22\text{ }\mu\text{m}$ at cloud top) is slightly larger and the droplet number concentrations
375 significantly lower (between 23 and 72 cm^{-3}). . Finally, **Jackson et al. (2012)** merged 41 MPC profiles during
376 the Indirect and Semi-Direct Aerosol Campaign (ISDAC) . They observed liquid droplet properties with mean
377 LWC around $0.15\text{ g}\cdot\text{m}^{-3}$ at cloud top, droplet size from 8 to $16\text{ }\mu\text{m}$ and droplet concentration around 150 cm^{-3} .
378 These results are consistent with our observations of the liquid phase within MPCs observed over the Greenland
379 and Norwegian Seas.

380

381 **3.2. Ice phase properties**

382

383 The ice crystal properties derived from the CPI measurements when the PN g-values are lower than 0.83 are
384 displayed on Figure 5 with the same representation as the one used for the liquid phase. In the following, the ice
385 crystal concentration corresponds to particles larger than $100\text{ }\mu\text{m}$ in order to minimize the effect of potential
386 shattering artifacts on this parameter (see **Febvre et al., 2012**). However, the extinction coefficient, the ice water
387 content, the effective diameter and particle size distribution are determined using all CPI images excluding those
388 identified as liquid droplets. This choice has been made to be consistent with previous studies and allow for
389 accurate comparisons with microphysical parameters obtained during Western Arctic campaigns. Averaged
390 values of ice crystal concentration (N_i) and extinction coefficient (σ_i) are around 3 L^{-1} and 0.4 km^{-1} respectively.
391 IWC and effective diameter ($D_{\text{eff},i}$) display mean values ranging from 0.01 to $0.035\text{ g}\cdot\text{m}^{-3}$ and from 80 to $130\text{ }\mu\text{m}$
392 respectively. No clear trend on the mean profiles of these properties is observed as no significant correlation with
393 height is found., However, the values of these parameters decrease to nearly zero at cloud top ($Z_n=1$). This
394 indicates that the cloud top layer is almost exclusively composed of supercooled liquid droplets and eventually a
395 very low concentration of small ice crystals as shown by the PSD on Fig 5e. These results corroborate the
396 findings from the previous experiments such as the ISDAC and M-PACE campaigns in Western Arctic

397 (McFarquhar et al., 2011; Jackson et al., 2012). These studies were based on 53 cloud profiles during the M-
398 PACE campaign (McFarquhar et al., 2011) and 41 cloud profiles during the ISDAC campaign (Jackson et al.,
399 2012). The ice crystal properties of single layer MPCs observed over the Beaufort Sea region did not show any
400 significant vertical variability.

401 Typical IWC and particle concentration (for crystals with size larger than $125\mu\text{m}$) values lied between 0.006 and
402 $0.025\text{ g}\cdot\text{m}^{-3}$ and between 1.6 L^{-1} and 5.6 L^{-1} for the M-PACE situations. These values are similar to those of the
403 COLD and WARM_NO cases of the present study. Averaged values of IWC and particle concentration during
404 ISDAC are in the range of the WARM_SO situations of the present work with values around $0.02\text{ g}\cdot\text{m}^{-3}$ and
405 0.27 L^{-1} respectively for the ISDAC situations. The average ice crystal size observed during M-PACE is around
406 $50\mu\text{m}$ which is smaller than the typical size found in our study. It could be explained by less efficient WBF and
407 riming processes and smaller droplet number also observed during M-PACE.

408 Deeper in the precipitation layer, closer to the sea level ($Z_n < -0.5$) no general trend can be depicted as ice
409 crystals properties show a large variability. Yet, no ice crystal were found in this region for the WARM_SO
410 situations, whereas the ice precipitation reaches the surface ($Z_n = -1$) for the COLD and WARM_NO regimes.

411 The particle shape vertical distribution was also investigated based on the CPI images. It can provide an insight
412 of the main microphysical growth processes occurring in such MPCs. Figure 6 displays the particle shape
413 distributions relative to number and mass concentration with Z_n (Figs. 6a and 6b) and temperature (Figs. 6c and
414 6d). To this purpose, particle shapes have been automatically classified by the algorithm developed at LaMP (see
415 details in Lefèvre, 2007). In addition, the resulting classification was supported by an accurate human-eye
416 visualization in order to control the results and avoid the main shortcomings linked to the automatic
417 classification. As indicated above, only particles with size greater than $100\mu\text{m}$ were taken into account in order
418 to avoid misclassification of smaller particles and shattering artifacts.

419 Our results clearly show that rimed and irregular ice crystals are dominant within MPCs (up to 80 % of the
420 total). In particular, irregular ice particles are encountered at all altitude and temperature. They account for 30 %
421 to 50 % of the total number concentration (and between 20 % and 30 % of mass concentration) depending on the
422 altitude or temperature of the MPC layer. Rimed particles are predominant inside the liquid containing cloud
423 layer ($0 < Z_n < 1$) with a contribution up to 40 % in number (60 % in mass) where low temperatures (below -18
424 $^{\circ}\text{C}$) are observed.

425 An interesting feature is the significant occurrence (around 40 %) of ice crystals with a predominant a-axis
426 growth at all cloud levels. Indeed, plates, sideplanes and stellars are the dominant habits among the regular
427 shapes regardless of the cloud layer altitude.

428 Below the cloud ($Z_n < 0$), precipitating ice crystals are characterized by a mass concentration dominated by
429 rimed particles and by large number concentration fraction of irregular ice crystals.

430 Over all, these results agree with the ones presented in McFarquhar et al. (2007) based on *in situ* observations
431 of MPCs during the M-PACE experiment. McFarquhar et al. also stated that small supercooled water droplets
432 dominated the upper layer of the cloud while larger ice particles were present in the lower part and below the
433 cloud (including irregular, aggregate or rimed-branched crystals). But our results differ since they observed a
434 fraction of needles and columns particles a lot larger than in our study (resp. up to 50% below the cloud versus
435 less than 10 %). On the opposite, our results are not in agreement with the observations described in Korolev et
436 al. (1999), this is because they observed even less regular ice crystals: irregular shaped ice crystals accounted for

437 up to 98 % of the total number of ice particles. This disagreement could be explained by two reasons. First,
438 **Korolev et al. (1999)** considered a wide variety of clouds sampled in the Canadian and US Arctic
439 (stratocumulus and cirrus at temperatures ranging from 0 to -45 °C and up to 7.5 km of altitude) whereas the
440 present study focuses only on MPCs in the Svalbard region at low altitudes. The disagreement may also stem
441 from the different image processing used in these studies. For instance, **Korolev et al. (1999)** took into account
442 particles larger than 40 μm (while a 100 μm threshold was used in our study) and two ice crystal shapes: pristine
443 (defined as faceted ice single particles) and irregulars were considered (while 10 particles shapes were accounted
444 for in our results).

446 3.3. Discussion on statistical vertical profiles

447
448 The quantitative estimates of the separate properties of droplets and ice crystals may give an insight on the
449 microphysical processes occurring in MPCs. These processes are involved in the MPC life cycle, in particular to
450 maintain the coexistence of liquid droplets and ice crystals, leading to its persistence (**Morrison et al., 2012**).
451 More specifically, the increase with height of droplet size and LWC observed in the vertical profiles is consistent
452 with a condensational growth process. The slight decrease on LWC and number concentration observed at the
453 very top of the cloud may be due to turbulent mixing (**Korolev et al., 2015**) and entrainment of dry air.
454 Additionally, the data collected in this part of the cloud may also lead to a slight underestimation of the LWC
455 since a mixing of cloudy and cloud free patches could be averaged together given the sampling resolution (i.e.
456 100 m). The analysis of the vertical profiles of ice properties and ice crystal shapes (cf. Fig .6) shows that the
457 presence of pristine particles, mainly plates and stellars could be linked to a very fast ice crystal growth by vapor
458 deposition due to Wegener-Bergeron-Findeisen process (WBF, **Bergeron, 1935; Findeisen, 1938; Wegener,**
459 **1911**) in which ice crystals grow at the expense of liquid droplets. The large contribution of rimed particles
460 confirmed that riming process shall be significant in a mixed phase cloud. The prevalence of irregular particles is
461 in agreement with the previous studies from **Korolev et al. (1999)** and **McFarquhar et al. (2007)** and suggests
462 that aggregation growth processes, or a combination of several growth mechanisms are involved. This also
463 indicates that turbulence or mixing into the cloud may have an important influence by redistributing the
464 precipitating ice crystals in the upper cloud levels. Measurements of the vertical wind speed (which are not
465 available for these campaigns) would be helpful to confirm this hypothesis.

466 Theoretical adiabatic LWC has also been determined assuming a non-entraining parcel of moist air rising and
467 reaching saturation. It is calculated from the pressure and temperature measurements from cloud base to cloud
468 top. These theoretical values are then compared to the observed LWC values to evaluate the influence of
469 turbulence or mixing effects on LWC as well as the efficiency of ice growth by WBF process or riming
470 processes. The profiles of the adiabatic ratio (the ratio of the adiabatic LWC to the observed LWC) are displayed
471 on Fig. 7. Subadiabatic values are found for all meteorological regimes. This means that processes responsible
472 for a decrease of LWC compared to the adiabatic prediction are prevalent. In particular, this strengthens the
473 assumption that a turbulent entrainment of dry air, resulting in the evaporation of liquid droplets, may occur at
474 cloud top. Moreover, this confirms that the WBF and riming processes are efficient and responsible for the
475 decrease of LWC compared to adiabatic values. These statements are in agreement with the study from (**Jackson**
476 **et al., 2012**) who showed for several boundary layer MPCs over Barrow, Alaska during the ISDAC campaign

477 that the subadiabatic profile of LWC and the decreasing droplet concentration at cloud top may be associated to
478 the ice crystal growth processes involving the liquid phase (riming and WBF) and/or the entrainment of dry air
479 from above.

480

481 However, Figs. 4 and 5 also showed significant differences in cloud vertical profiles from one regime to another.
482 The COLD situations exhibit the largest values for ice properties (IWC up to 0.075 g.m^{-3} , N_i up to 8 L^{-1}) together
483 with the lowest LWC values ($< 0.1 \text{ g.m}^{-3}$). On the contrary, the WARM_SO profiles are characterized by the
484 largest liquid droplet concentrations, extinction coefficient and LWC values ($\sim 200 \text{ cm}^{-3}$, 40 km^{-1} and 0.3 g.m^{-3}
485 respectively) and low values of IWC, extinction and size of ice crystals ($\text{IWC} < 0.01 \text{ g.m}^{-3}$, $\sigma_i < 0.2 \text{ km}^{-1}$ and D_{eff}
486 $< 50 \text{ }\mu\text{m}$ respectively). Thus in the WARM_SO regime, it seems that the ice crystal number is too low and their
487 size too small to efficiently consume liquid droplets by WBF or riming processes (**Pruppacher and Klett,**
488 **1978**), explaining on one hand the prevalence of the liquid phase and the other hand that the precipitating ice
489 crystal below the cloud do not reach the surface. Moreover, the habit classification as a function of the
490 temperature shows differences between the COLD regime and the WARM regimes (not shown here). This
491 concern in particular the presence of some large droplets in the WARM regimes which are not present in the
492 COLD regime, and the presence of plate and stellar particles below -10°C or around -4°C , which is consistent
493 with the classical ice crystal morphology diagram ((**Libbrecht, 2005; Nakaya, 1954**).

494 The adiabatic ratio, shown in Figure 7, confirms this assumption where larger values are encountered for the
495 WARM_SO situations. Indeed, a large adiabatic ratio denotes that processes responsible for the depletion of
496 liquid droplets (mainly riming or WBF) are relatively less efficient.

497 The ice crystal properties relative to the WARM_NO situations are similar to the WARM_SO cases, except for
498 the effective diameter where values are similar to the COLD regime ($D_{\text{eff},i} > 100 \text{ }\mu\text{m}$). The liquid droplets for this
499 regime exhibit the lowest concentrations ($< 100 \text{ cm}^{-3}$), and intermediate LWC value (around 0.2 g.m^{-3}).

500

501 The meteorological classification used in our study is also based on the air mass origin since it shall impact the
502 cloud microphysical properties, as shown in **Gultepe and Isaac (2002)**. In particular COLD and WARM_NO
503 situations characterized by northern air mass origin should be associated to more pristine conditions and drier air
504 compared to the WARM_SO situations. Airborne *in situ* aerosol measurements were only available during the
505 POLARCAT 2008 campaign (with particle counters). However nearly continuous aerosol measurements (with
506 particle counters and sizers) but ground based were performed at the Mountain Zeppelin station (Ny-Alesund,
507 Svalbard 475 m above sea level, 79°N , 12°E) during a period encompassing the ASTAR and SORPIC
508 campaigns. Even though, these measurements do not provide an accurate estimate of the aerosol concentration at
509 the exact location and time when the clouds were sampled, it still give an indication on the background aerosol
510 loading. Based on these measurements, the mean aerosol number concentrations were 230, 120 and 330 cm^{-3} for
511 the COLD, WARM_NO and WARM_SO respectively we can conclude that pristine conditions are encountered
512 for air masses originating from the North, and that cloud measurements performed under WARM_SO conditions
513 are more likely to be affected by long range transport of pollution for the South/East.

514 The prevalence of the ice phase for the COLD regime is thus consistent both with the cold temperature and the
515 pristine conditions associated with Northern air masses. Despite similar air mass origins, the WARM_NO cases
516 exhibit smaller concentration of ice crystals than the COLD situations. This suggests that the influence the cloud

517 top temperature prevails to promote the growth or production of ice crystals. The WARM_SO cases which
518 combine warm temperatures and continental air masses clearly shows that the ice crystal growth or production is
519 reduced, as well as the precipitation efficiency, and that the liquid phase dominates the cloud structure.
520 Additionally, the comparison of the vertical profiles of MPC properties of the present work to the previous
521 studies concerning the Western Arctic in section 3.2 showed that the cloud properties for the COLD and
522 WARM_NO situations agree with that of M-PACE (REF), in particular in terms of ice concentration and IWC.
523 The WARM_SO cases agree more with the ISDAC situations, in particular the low ice concentration. **Jackson**
524 **et al. (2012)** explained the very low ice concentration observed during ISDAC as a consequence of more
525 polluted situations encountered (compared to M-PACE) that might reduce the secondary ice crystal production
526 efficiency (thermodynamic indirect effect). This conclusion is thus in accordance with our assumption that the
527 air mass coming from the South may be more impacted by pollution and may reduce the ice growth efficiency.
528 These analysis show that microphysical properties of arctic MPCs over the Greenland and Norwegian seas are
529 closely linked to the cloud top temperature regime and the environmental conditions such as the air mass origin.
530 Similar conclusions have already been made for MPCs in the western Arctic regions by **Gultepe and Isaac**
531 **(2002)** who demonstrated the impact of the air mass origin (Pacific Ocean or Arctic Ocean) on the MPC
532 microphysical properties.
533 However, a more thorough analysis involving collocated *in situ* aerosols measurements are obviously needed to
534 comfort these findings. For instance, our results are somehow consistent with **Lance et al. (2011) or Rangno**
535 **and Hobbs (2001)** who showed that “polluted” MPCs exhibit higher droplet concentrations and smaller ice
536 precipitating particles compared to “clean” MPCs. A large number of droplets is expected to reduce the riming
537 process and thus contribute to the large observed values of LWC (as liquid droplets are not consumed by the ice
538 crystals).

539
540 To go further into the analysis of our microphysical dataset, additional measurements of key parameters are
541 necessary. In particular, quantifying the mechanisms responsible for the formation and growth of droplets and
542 ice crystals within MPCs by measuring the numbers of ice nuclei (IN) and CCN are needed. It would enable us
543 to perform an accurate ice closure and to quantify for example the possible impact of secondary ice production
544 process). A better characterization of the dynamical processes at cloud scale, with accurate high spatial
545 resolution measurements of vertical wind velocities into and around the MPCs would also be necessary. For
546 instance, upward air motion and turbulent entrainment of air from above the cloud are critical to maintain liquid
547 water in MPCs. Accurate humidity measurements would also be needed to better identify condensational growth
548 of ice crystals (WBF process or direct condensation of water vapor on ice, as described by **Korolev (2007)**) and
549 resolve the issue of turbulence and mixing at cloud edges and into cloud. All these parameters, along with
550 radiative flux measurements, are of primary importance to constrain our assumptions on the microphysical
551 processes.

552 At last, coupling our results (and further observations with new parameters and improved instrumentation) with
553 modeling is of course the best way to quantify the relative impact of each process on the MPC lifetime. But such
554 a work remains beyond the scope of the present study.

555

556 4. Parameterizations of key microphysical parameters

557

558 In section 3, we have shown that *in situ* data provide a detailed characterization of the microphysical and optical
559 properties of MPCs. These measurements can also be used to develop cloud parameterizations and to evaluate
560 remote sensing retrieval products or modeling outputs. This section focuses on the key properties and hence
561 parameters which must be better quantified (**Morrison and Pinto, 2006**), namely: (i) IWC (and LWC) –
562 extinction coefficient relationships, (ii) the variability of the ice and liquid water paths, (iii) the temperature
563 dependent ice crystal concentration and (iv) the liquid water fraction (ratio of LWC over total water content) as a
564 function of the cloud level or temperature.

565

566 **4.1. Ice and liquid water contents and integrated paths**

567

568 Linking cloud microphysical and optical properties is an important step in order to model the cloud radiative
569 properties or to constrain/develop remote sensing retrieval methods. In particular, accurate IWC-extinction
570 relationships and integrated properties such as ice and liquid water paths are needed to improve the remote
571 sensing retrieval products and cloud modeling (**Heymsfield et al., 2005; Waliser et al., 2009**). In this section,
572 we provide such relationships and parameters based on *in situ* measurements.

573

574 Figures 8a and 8b display the IWC and the LWC measurements as a function of the ice and droplet extinction
575 coefficients respectively, with the temperature superimposed in color. The averaged values of IWC and LWC
576 over intervals of 0.1 km^{-1} and 2 km^{-1} for the ice and liquid extinction coefficient respectively are represented by
577 the grey squares in order to determine the fitting curves (represented by the red lines with the mean absolute
578 error in dashed lines). Ice crystals and liquid droplets extinction coefficients are well correlated with their water
579 content counterparts. The correlation coefficients are high (0.88 for ice and 0.90 for liquid) and the IWC- σ and
580 LWC- σ relationships are nearly linear.

581 It should also be noted that including the temperature as an additional parameter for the linear fitting did not
582 improve the accuracy of the parameterizations, contrary to previous studies of **Heymsfield et al. (2005)**, **Hogan**
583 **et al. (2006)**, or **Protat et al. (2007, 2016)**. However these previous studies concerned tropical and mid-latitude
584 clouds and cover a much broader range of temperatures (from -65°C to 0°C , compared to narrower range from
585 24°C to 0°C in our study).

586

587 Integrated properties such as LWP and IWP are common modeling outputs which suffer from large
588 discrepancies depending on the model specifications (**Waliser et al., 2009**). Moreover only a very limited
589 number of studies were devoted to retrieve these properties from *in situ* measurements in this region of the
590 Arctic. Since the flight legs selected in our study target ascending and descending sequences into single-layer
591 MPCs, *in situ* measurements can be used to determine IWP and LWP according to the following equation:

592

$$593 \text{IWP (or LWP)} = \int_{\text{ground}}^{\text{cloud top}} \text{IWC (or LWC)}(z) dz \quad (3)$$

594

595 We recall that these integrated properties should be considered as quasi-instantaneous as ascending and
596 descending flight sequences are obviously not fully vertical and need about 5-10 minutes to be performed
597 (compared to the snapshots performed by remote sensing measurements).

598

599 Figure 8c displays the ice (green) and liquid (blue) water paths as a function of the cloud top temperature (1 °C
600 intervals). For cloud top temperatures below -20 °C, IWP and LWP reach values close to 30 g.m⁻² and 50 g.m⁻²
601 respectively. The IWP decreases dramatically when the cloud top temperature increases: to very low values close
602 to 0 are encountered at temperatures above -8 °C. LWP reaches a maximum of 100 g.m⁻² at -13 °C and the
603 smallest values (around 15 g.m⁻²) are encountered when the cloud top temperature is typically around -18°C.
604 These findings are consistent with the main previous studies devoted to Arctic MPCs from (**Hobbs et al., 2001;**
605 **Pinto, 1998; Pinto and Curry, 2001; Shupe et al., 2006**). They reported mean LWP values in the range of 20-
606 70 g.m⁻², with some maxima up to around 130 g.m⁻², and IWP mean values less than 40 g.m⁻². However, one
607 shall note that all these previous studies concerned once again the MPCs in the western Arctic regions (Barrow,
608 Alaska, Beaufort Sea).

609

610 4.2. Ice crystal concentration

611

612 The accurate knowledge of the ice crystal concentration is of primary importance to correctly parameterize the
613 initiation and evolution of the ice phase in models, and reduce the significant uncertainties in the modelling of
614 the ice/liquid partitioning within MPCs.

615 Figure 9 shows the maximum number concentration of ice crystals with size greater than 100 µm as a function of
616 the cloud top temperature for each MPC vertical profile. The data points are color-coded according the COLD,
617 WARM_NO and WARM_SO environmental regimes. This figure highlights that the maximum ice
618 concentration varies almost exponentially (figure is in log-lin scale) with the cloud top temperature, with
619 nevertheless a large variability. Thus, a relationship may be fitted in order to parameterize the ice crystals
620 number concentration as a function of temperature in MPCs (equation included in Fig. 9), even though the
621 correlation coefficient is quite low (0.43). The mean absolute error (MAE) is also displayed on figure 10 (dotted
622 lines) to estimate the uncertainties on the parameterization. For comparison purposes, the parameterizations of
623 **Meyers et al. (1992)** and **Cooper (1986)** for heterogeneous ice nucleation and the parameterization of **Young et**
624 **al. (2017)** for primary ice nucleation based on microphysical observations during the Aerosol-Cloud Coupling
625 and Climate Interactions in the Arctic (ACCACIA) campaign are displayed (in purple, orange and brown dashed
626 lines respectively). The **Meyers et al. (1992)** parameterization is within the range of the uncertainties of our
627 parameterization. However it significantly deviates from our relationship for cloud top temperature higher than -
628 15°C i.e. for clouds under warm regime. For these regimes the ice number concentrations can differ by a factor
629 up to two at -10°C.

630 The parameterizations of **Cooper (1986)** and **Young et al. (2017)** do not match with the present
631 parameterization since the ice crystal concentrations predicted are around one order of magnitude lower than the
632 ones in the present study. This difference can be explained by the different seasons, cloud types and locations of
633 the observations used for the parameterization of **Cooper (1986)** and the fact that the range of their measured
634 concentrations lie within a factor of 10 as they noted.

635 In contrast, the sampling conditions for the determination of the **Young et al. (2017)** parameterization are more
636 similar to the present work, they used measurements in Arctic MPCs over the Greenland Sea. The dataset was
637 collected during spring and summer, above open sea, ice sheet and transitions. This variability in the seasons and
638 surface conditions may explain the differences observed compared to the present work. Above all, **Young et al.**
639 **(2017)** displayed an averaged concentration whereas the maximum ice number is presented here. But even by
640 taking the averaged ice concentrations in the present work, the parameterization does not match with that of
641 **Young et al. (2017)** (not shown here). Finally, the detailed time series displayed in the **Young et al. (2016)** and
642 **Lloyd et al. (2015)** works which present the cases used for the determination of the parameterization of **Young**
643 **et al. (2017)** showed that the maximum ice number concentrations frequently displayed values between 1 L^{-1} and
644 5 L^{-1} which is in the range of the present parameterization.

645 Our results could not be compared to more sophisticated parameterizations accounting for supersaturation and
646 aerosol properties (such as **(DeMott et al., 2011)** since additional data are needed (aerosol and CCN/IN
647 measurements, humidity). These additional data are also necessary to discuss the processes such as the secondary
648 ice production processes which could explain the higher crystal numbers observed in the present study compared
649 to the other works presented in this section.

650

651

652 **4.3. Liquid water fraction**

653

654 The MPC liquid fraction can be determined based on the separate liquid and ice properties presented in section
655 3. The liquid water fraction (hereafter LWF) is defined as the ratio of liquid water content LWC over the total
656 water content TWC ($\text{IWC} + \text{LWC}$) at each altitude level.

657 To our knowledge very few previous studies have assessed the liquid water fraction in MPCs. Most of them
658 concerned MPCs only in western Arctic regions (**de Boer et al., 2009; McFarquhar et al., 2007; Shupe et al.,**
659 **2006**).

660 Figure 10a displays the liquid fraction according to the normalized altitude. For purpose of comparisons, the
661 parameterization from **McFarquhar et al. (2007)** (hereafter MF07) determined from *in situ* measurements
662 during M-PACE is also represented on Fig. 10a by the black dotted curve. Our relationship significantly deviates
663 from that of MF07. They used *in situ* measurements from 53 profiles in single layer MPCs sampled over Alaska
664 with temperatures ranging from $-3 \text{ }^{\circ}\text{C}$ to $-17 \text{ }^{\circ}\text{C}$. As mentioned in section 3 they observed similar ice crystal
665 number concentrations but ice crystals smaller with mean effective diameters around $50 \text{ }\mu\text{m}$ compared to 100
666 μm in our study.

667 Figure 10b shows the liquid fraction according to cloud top temperature. Each point represents the mean value of
668 the liquid fraction determined for each profile. The error bars corresponding to the standard deviation display
669 large values around 80 % indicative of a large variability. Nevertheless, Fig. 10b shows that LWF is well
670 correlated with the cloud top temperature. The decrease in LWF associated with a decrease of temperature is
671 consistent with Fig. 9 which shows that ice number concentration increases for colder temperatures.

672 The liquid fraction is also determined at each cloud level as a function of the temperature on Fig. 10c (with $1 \text{ }^{\circ}\text{C}$
673 temperature interval). The same trend as in Fig. 10a is observed. The liquid water fraction increases with
674 decreasing temperature. The relationship between LWF and T is nearly linear with similar slopes for the three

675 regimes. However, large shifts are observed from one regime to another, especially when comparing the COLD
676 regime to the WARM_NO and the WARM_SO. This shift is clearly linked to the temperature profiles (see Fig.
677 3). However, one can note that the results for the WARM_NO regime are the ones in the closest agreement with
678 the MF07 parameterization.

679 In order to compare our results to those of **Shupe et al. (2006)**, we also determined the total liquid water fraction
680 (LWF_{total}) in terms of water paths (LWP/TWP). Fig. 10d shows a rather good agreement between the two water
681 path ratios, showing that IWP dominates in the coldest clouds (T_{top} around -20 °C in average). On the opposite,
682 LWF_{total} is more important in the warmer MPCs (T_{top} above -15 °C). However such liquid fraction determination
683 must be taken with care since it integrates the ice region below the clouds (**de Boer et al., 2009**).

684
685

686 5. Conclusions and outlook

687

688 In this study, a characterization of Arctic boundary-layer mixed phase clouds microphysical properties has been
689 performed. *In situ* data from 4 airborne campaigns over the Greenland Sea and the Svalbard region are compiled
690 and analyzed. The data set represents in total 18 flights and 71 vertical profiles in MPCs (more than 350 minutes
691 of cloud *in situ* observations). Cloud phase discrimination is achieved and vertical profiles of number, size, mass
692 and shapes of ice crystals and liquid droplets within MPCs are determined.

693

694 The main conclusions of the present work are summarized as follow:

695

696 i) Liquid phase is mainly present in the upper part of the MPCs with high concentration of small
697 droplets ($N_w \sim 120 \text{ cm}^{-3}$, $D_{eff,w} \sim 15 \text{ }\mu\text{m}$), and averaged LWC around $0.2 \text{ g}\cdot\text{m}^{-3}$. Ice crystals are
698 present everywhere in the MPCs with no significant vertical variability ($N_i \sim 3 \text{ L}^{-1}$, $D_{eff,i} \sim 100$
699 μm , $IWC \sim 0.025 \text{ g}\cdot\text{m}^{-3}$), but mainly in the lower part, and precipitate down to the surface. The
700 morphology study of ice crystals images showed that irregular and rimed particles prevail over
701 stellars and plates habits.

702

703 ii) The vertical profiles of the microphysical properties and the shape distribution can also be
704 used to give an insight of the microphysical processes occurring in MPCs. It is likely that
705 adiabatic lifting (condensation) is the main process for liquid droplets initiation and growth,
706 and that evaporation at cloud top due to entrainment of dry air seems to occur. In the cloud
707 layer, where liquid droplets and ice crystals coexist, Wegener-Bergeron-Findeisen and riming
708 processes are the main mechanisms involved in the ice crystal growth. The large occurrence of
709 irregular particles highlights the fact that the ice crystals undergo a variety of growth
710 processes, and the turbulence in the MPCs life cycle is efficient to mix the cloud.

711

712 iii) The analysis of the scattering phase function showed a very high correlation between optical
713 properties and liquid to ice fraction within the MPC layers.

714

715 iv) Statistical analysis exhibits significant differences in the vertical profiles of MPC properties
716 depending if the cloud top is cold or warm and if the air mass has its origin from higher or
717 lower latitudes. The largest droplet concentration and LWC values observed (200 cm^{-3} , 0.3
718 g.m^{-3} respectively) are associated with the warm temperature regime with air mass originating
719 from the South/East (continental areas). For these situations, at the same time, very low values
720 of ice crystal size and IWC are observed ($\text{IWC} < 0.01 \text{ g.m}^{-3}$, $D_{\text{eff},i} \sim 50 \mu\text{m}$). On the opposite,
721 the colder situations exhibit large values of ice contents especially when air masses originate
722 from the North ($\text{IWC} \sim 0.075 \text{ g.m}^{-3}$). These results underline the importance of the air mass
723 origin and the cloud top temperature as well as the need of simultaneous aerosol measurements
724 (sources, transport, physical and chemical properties) in connection with the MPC properties
725 to study the cloud-aerosol interactions and improve the understanding of ice and liquid
726 formation processes.

727 v) The main results of the present work were compared to the previous studies which concern
728 mainly MPCs in the Western Arctic region. The main findings showed that the properties of
729 the COLD and WARM_NO situations (large values of ice properties) of the present work are
730 consistent with the rather clean situations of previous Western Arctic studies such as M-PACE.
731 On the opposite, the MPC properties of the WARM_SO cases (prevalence of liquid phase and
732 very low values of ice properties) are more in agreement with the more polluted situations in
733 Western Arctic, such as ISDAC. These findings confirm that the MPC properties are strongly
734 linked to the environmental conditions such as temperature and air mass origin.

735 vi) Several parameterizations for remote sensing or modeling are proposed. It concerns the
736 determination of IWC (and LWC) – extinction relationships, ice and liquid integrated water
737 paths, the ice concentration and liquid water fraction. Comparisons with the few previous
738 works available in the literature showed in general a good agreement. Obviously, the
739 application range of the established relationships is only for Arctic MPCs and temperature
740 range between 0 and $-23 \text{ }^\circ\text{C}$. A next step to the present work will be to apply the proposed
741 parameterizations to remote sensing algorithms and modelling to investigate their relevance.

742
743
744
745
746 This study provided for the first time a statistical analysis of Arctic MPC *in situ* data from 4 airborne campaigns
747 located in the Eastern Arctic region. An accurate characterization of the vertical variability of liquid droplets and
748 ice crystals properties has been made, allowing the development of parameterizations.

749 Further studies should involve new measurement technic to provide accurate characterization of cloud phase and
750 microphysical properties, in particular for the small particles. This will allow to complete and validate the
751 present results. For example, instruments like the small ice detector (SID-3, **Ulanowski et al., 2014; Vochezer**
752 **et al., 2016**) or the cloud particle spectrometer with polarization detection (CPSPD, **Baumgardner et al. (2014)**)
753 should provide valuable measurements to differentiate droplets from ice crystal even at size lower than $50\mu\text{m}$.
754 Both probes are open path to avoid shattering artefacts. Additionally, accurate measurements of humidity and
755 aerosol (CCN and IN) remains an important shortage in order to deep the analysis of microphysical processes

756 and to realize ice and liquid closure and better understand life cycle and persistence of such particular clouds. In
 757 this purpose, a modeling study of cloud microphysics shall be of help. Finally, by characterizing clouds at very
 758 low altitude levels, this work can be useful in future studies for validate/evaluate space remote sensing
 759 observations and retrieval products (A-Train, EarthCare...) since these measurements are known to have
 760 important shortcomings near the surface.

761

762

763 **Appendix A: Data processing of *in situ* measurements**

764

765 The methodology developed by **Lawson and Baker (2006)** to derive the Ice Water Content (IWC) from 2D
 766 particle images recorded by the CPI instruments is applied (Eq. (A1) below).

$$767 \quad IWC = \frac{0.135 \sum_i X_i^{0.793}}{V} \quad (A1)$$

768 where V is the sample volume and X_i is the mass parameter for each crystal image defined by Lawson and Baker
 769 (2006) as follow:

$$770 \quad X_i = \frac{A_i \times W_i \times 2 \times (L_i + W_i)}{P_i} \quad (A2)$$

771 A_i , W_i , L_i and P_i are the area, width, length and perimeter of the crystal image i .

772

773 The extinction coefficient (σ) and the effective diameter (D_{eff}) are determined from CPI and FSSP measurements
 774 as follow:

$$775 \quad \sigma_{ice \text{ (or liquid)}} = 2 \times \frac{\sum_i A_i}{V} \quad (A3)$$

$$776 \quad D_{eff,ice \text{ (or liquid)}} = C \times \frac{IWC \text{ (or LWC)}}{\sigma_{ice \text{ (or liquid)}}} \quad (A4)$$

777 with constant $C = 3000 \text{ mm}^3 \cdot \text{g}^{-1}$ according to **Gayet et al. (2002)**.

778 The LWC derived from the Nevzorov probe measurements is calculated according to **Korolev et al. (1998)** :

779

$$780 \quad LWC_{Nevzorov} = \frac{P_{LWC} - \left(\frac{P_{TWC} \times \epsilon_{LWC,i} \times S_{LWC}}{\epsilon_{TWC,i} \times S_{TWC}} \right)}{L_v \times S_{LWC} \times U \times \left(\epsilon_{LWC,l} - \frac{\epsilon_{LWC,i} \times \epsilon_{TWC,l}}{\epsilon_{TWC,i}} \right)} \quad (A5)$$

781

782 where P_{LWC} and P_{TWC} are the power supplied to the LWC and TWC sensors to maintain the constant temperature
783 of the wire.

784 S_{LWC} and S_{TWC} are the surface of the sensors, L_v is the latent heat of vaporization and U is the true airspeed.

785 The epsilon terms refer to the collection efficiencies of liquid droplets (l index) or ice crystals (i index) on the
786 LWC and TWC sensors. These efficiencies are set as follow:

787 $\epsilon_{LWC,l} = 0.76$: see **Schwarzenboeck et al. (2009)**;

788 $\epsilon_{LWC,i} = 0.11$: following **Korolev et al. (1998)**;

789 $\epsilon_{TWC,l} = 1$: according to **Korolev et al. (1998)** for droplets with size around 25 μm ;

790 $\epsilon_{TWC,i} = 1$: following **Schwarzenboeck et al. (2009)**. It should be noticed that taking $\epsilon_{TWC,i} = 3$ (as
791 assumed in **Korolev et al., 2013**) instead of 1 induces an increase of LWC by 10 % only.

792 The uncertainties associated to the microphysical and optical properties derived from FSSP-100, PN, Nevzorov
793 and CPI measurements are detailed in (**Baumgardner and Spowart, 1990**; **Gayet et al., 2002**; **Korolev et al.,**
794 **1998**; **Mioche, 2010**) respectively, and are summarized in Table 2.

795 **Appendix B: Effects of shattering of ice crystals on measurements**

796 Techniques and methods exist now to avoid or estimate this shattering effect, such as new-designed inlets or
797 measurements of the particles inter-arrival time (**Field et al., 2003**), but none of these were available for this
798 study. However in order to assess the accuracy of the present dataset and highlight a possible impact of
799 shattering effect, a brief intercomparison of the extinction coefficient from the three data sets was conducted.
800 Indeed, the extinction coefficient is the only parameter which can be derived by the measurements of the three
801 probes. Moreover, it is not determined with the same method, since it is calculated from the PSD for the CPI and
802 the FSSP, and from the scattering phase function for the PN. One more important point is that CPI, FSSP and PN
803 have all different size inlets (23 mm, 40 mm and 10 mm diameter respectively). So, from these information, we
804 could assume that, if shattering effect is present on ice particles, its magnitude (i.e. the number of smaller new
805 artifact particles) would differ from one instrument to another. Thus, the comparison of the extinction coefficient
806 from CPI, FSSP and PN measurements would highlight such discrepancies.

807 Figure B1 displays the comparison of the extinction coefficient derived from the PN and from the combination
808 of the CPI and FSSP for all the *in situ* data available for this study. Note that the combination of CPI and FSSP
809 data covers the same size range of the PN. Figure B1 clearly shows that the extinction coefficient measurements
810 derived from the combination of the CPI and FSSP and the PN are very well correlated (with a coefficient of
811 0.87) and no significant bias is observed (regression coefficient of 0.98). Thus, since the design of the
812 instruments and data processing are different for each dataset, these results highlight that the shattering effect is
813 probably smaller than the measurements uncertainties (25 %, 35 % and 55 % for PN, FSSP and CPI respectively,
814 see Table 2).

815 **Acknowledgments**

816 This research was funded by the Centre National de la Recherche Scientifique – Institut National des Sciences de
817 l’Univers (CNRS-INSU) and the Expecting EarthCare Learning from A-Train (EECLAT) project. We thank the
818 Alfred Wegener Institute (AWI) and the Service des Avions Français Instrumentés pour la Recherche en

819 Environnement (SAFIRE) for the organization of the campaigns and for providing research aircrafts. The authors
820 acknowledge the NOAA Air Resources Laboratory (ARL) for the provision of the HYSPLIT transport and
821 dispersion model and READY Web site (<http://www.arl.noaa.gov/ready.html>) used in this publication. We
822 thank Peter Tunved from the Stockholm University for providing via the EBAS database the aerosol data from
823 Mount Zeppelin station. We thank anonymous reviewers who made very useful comments to strengthen the
824 manuscript.
825

826 **References**

- 827 Avramov, A. and Harrington, J. Y.: Influence of parameterized ice habit on simulated mixed
828 phase Arctic clouds, *J. Geophys. Res.*, 115(D3), doi:10.1029/2009JD012108, 2010.
- 829 Avramov, A., Ackerman, A. S., Fridlind, A. M., van Diedenhoven, B., Botta, G., Aydin, K.,
830 Verlinde, J., Korolev, A. V., Strapp, J. W., McFarquhar, G. M., Jackson, R., Brooks, S. D.,
831 Glen, A. and Wolde, M.: Toward ice formation closure in Arctic mixed-phase boundary layer
832 clouds during ISDAC, *J. Geophys. Res.*, 116(D00T08), doi:10.1029/2011JD015910, 2011.
- 833 Baker, B. and Lawson, R. P.: Improvement in Determination of Ice Water Content from Two-
834 Dimensional Particle Imagery. Part I: Image-to-Mass Relationships, *J. Appl. Meteorol.*
835 *Climatol.*, 45(9), 1282–1290, doi:10.1175/JAM2398.1, 2006.
- 836 Baumgardner, D. and Spowart, M.: Evaluation of the Forward Scattering Spectrometer Probe.
837 Part III: Time Response and Laser Inhomogeneity Limitations, *J. Atmospheric Ocean.*
838 *Technol.*, 7(5), 666–672, doi:10.1175/1520-0426(1990)007<0666:EOTFSS>2.0.CO;2, 1990.
- 839 Baumgardner, D., Gayet, J.-F., Gerber, H., Korolev, A. V. and Twohy, C.:
840 Clouds/Measurement Techniques In Situ, in: *Encyclopedia of Atmospheric Sciences*, in
841 *Encyclopedia of Atmospheric Sciences*, p. 4000, Holton, J. R., Curry, J. A., and Pyle, J.,
842 London., 2002.
- 843 Baumgardner, D., Avallone, L., Bansemer, A., Borrmann, S., Brown, P., Bundke, U., Chuang,
844 P. Y., Cziczko, D., Field, P., Gallagher, M., Gayet, J.-F., Heymsfield, A., Korolev, A., Krämer,
845 M., McFarquhar, G., Mertes, S., Möhler, O., Lance, S., Lawson, P., Petters, M. D., Pratt, K.,
846 Roberts, G., Rogers, D., Stetzer, O., Stith, J., Strapp, W., Twohy, C. and Wendisch, M.: In
847 Situ, Airborne Instrumentation: Addressing and Solving Measurement Problems in Ice
848 Clouds, *Bull. Am. Meteorol. Soc.*, 93(2), ES29-ES34, doi:10.1175/BAMS-D-11-00123.1,
849 2012.
- 850 Baumgardner, D., Newton, R., Krämer, M., Meyer, J., Beyer, A., Wendisch, M. and
851 Vochezer, P.: The Cloud Particle Spectrometer with Polarization Detection (CPSPD): A next
852 generation open-path cloud probe for distinguishing liquid cloud droplets from ice crystals,
853 *Atmospheric Res.*, 142, 2–14, doi:10.1016/j.atmosres.2013.12.010, 2014.
- 854 Bergeron, T.: On the physics of clouds and precipitation, *Int. Union Geod. Geophys.*, 156–
855 178, 1935.
- 856 Bierwirth, E., Ehrlich, A., Wendisch, M., Gayet, J.-F., Gourbeyre, C., Dupuy, R., Herber, A.,
857 Neuber, R. and Lampert, A.: Optical thickness and effective radius of Arctic boundary-layer
858 clouds retrieved from airborne nadir and imaging spectrometry, *Atmospheric Meas. Tech.*,
859 6(5), 1189–1200, doi:10.5194/amt-6-1189-2013, 2013.

860 de Boer, G., Eloranta, E. W. and Shupe, M. D.: Arctic Mixed-Phase Stratiform Cloud
861 Properties from Multiple Years of Surface-Based Measurements at Two High-Latitude
862 Locations, *J. Atmospheric Sci.*, 66(9), 2874–2887, doi:10.1175/2009JAS3029.1, 2009a.

863 Chernokulsky, A. and Mokhov, I. I.: Climatology of Total Cloudiness in the Arctic: An
864 Intercomparison of Observations and Reanalyses, *Adv. Meteorol.*, 2012, 1–15,
865 doi:10.1155/2012/542093, 2012.

866 Cober, S. G., Isaac, G. A., Korolev, A. V. and Strapp, J. W.: Assessing Cloud-Phase
867 Conditions, *J. Appl. Meteorol.*, 40(11), 1967–1983, doi:10.1175/1520-
868 0450(2001)040<1967:ACPC>2.0.CO;2, 2001.

869 Cooper, W. A.: Ice Initiation in Natural Clouds, *Meteorol. Monogr.*, 21(43), 29–32,
870 doi:10.1175/0065-9401-21.43.29, 1986.

871 Curry, J. A.: Interactions among aerosols, clouds, and climate of the Arctic Ocean, *Sci. Total*
872 *Environ.*, 160–161, 777–791, doi:10.1016/0048-9697(95)04411-S, 1995.

873 Curry, J. A., Schramm, J. L., Rossow, W. B. and Randall, D.: Overview of Arctic Cloud and
874 Radiation Characteristics, *J. Clim.*, 9(8), 1731–1764, doi:10.1175/1520-
875 0442(1996)009<1731:OOACAR>2.0.CO;2, 1996.

876 de Boer, G., Eloranta, E. W. and Shupe, M. D.: Arctic Mixed-Phase Stratiform Cloud
877 Properties from Multiple Years of Surface-Based Measurements at Two High-Latitude
878 Locations, *J. Atmospheric Sci.*, 66(9), 2874–2887, doi:10.1175/2009JAS3029.1, 2009b.

879 Delanoë, J., Protat, A., Jourdan, O., Pelon, J., Papazzoni, M., Dupuy, R., Gayet, J.-F. and
880 Jouan, C.: Comparison of Airborne In Situ, Airborne Radar–Lidar, and Spaceborne Radar–
881 Lidar Retrievals of Polar Ice Cloud Properties Sampled during the POLARCAT Campaign, *J.*
882 *Atmospheric Ocean. Technol.*, 30(1), 57–73, doi:10.1175/JTECH-D-11-00200.1, 2013.

883 DeMott, P. J., Möhler, O., Stetzer, O., Vali, G., Levin, Z., Petters, M. D., Murakami, M.,
884 Leisner, T., Bundke, U., Klein, H., Kanji, Z. A., Cotton, R., Jones, H., Benz, S., Brinkmann,
885 M., Rzesanke, D., Saathoff, H., Nicolet, M., Saito, A., Nillius, B., Bingemer, H., Abbatt, J.,
886 Ardon, K., Ganor, E., Georgakopoulos, D. G. and Saunders, C.: Resurgence in Ice Nuclei
887 Measurement Research, *Bull. Am. Meteorol. Soc.*, 92(12), 1623–1635,
888 doi:10.1175/2011BAMS3119.1, 2011.

889 Dong, X., Xi, B., Crosby, K., Long, C. N., Stone, R. S. and Shupe, M. D.: A 10 year
890 climatology of Arctic cloud fraction and radiative forcing at Barrow, Alaska, *J. Geophys.*
891 *Res.*, 115(D17212), doi:10.1029/2009JD013489, 2010.

892 Draxler, R. R. and Rolph, G. D.: HYSPLIT (HYbrid Single-Particle Lagrangian Integrated
893 Trajectory) model access via NOAA ARL READY website (<http://www.arl.noaa.gov/ready/hysplit4.html>), 2003.

894

895 Ehrlich, A., Wendisch, M., Bierwirth, E., Gayet, J.-F., Mioche, G., Lampert, A. and Mayer,
896 B.: Evidence of ice crystals at cloud top of Arctic boundary-layer mixed-phase clouds derived
897 from airborne remote sensing, *Atmospheric Chem. Phys.*, 9(24), 9401–9416, doi:10.5194/acp-
898 9-9401-2009, 2009.

- 899 Eidhammer, T., DeMott, P. J., Prenni, A. J., Petters, M. D., Twohy, C. H., Rogers, D. C.,
900 Stith, J., Heymsfield, A., Wang, Z., Pratt, K. A., Prather, K. A., Murphy, S. M., Seinfeld, J.
901 H., Subramanian, R. and Kreidenweis, S. M.: Ice Initiation by Aerosol Particles: Measured
902 and Predicted Ice Nuclei Concentrations versus Measured Ice Crystal Concentrations in an
903 Orographic Wave Cloud, *J. Atmospheric Sci.*, 67(8), 2417–2436,
904 doi:10.1175/2010JAS3266.1, 2010.
- 905 Febvre, G., Gayet, J.-F., Shcherbakov, V., Gourbeyre, C. and Jourdan, O.: Some effects of ice
906 crystals on the FSSP measurements in mixed phase clouds, *Atmospheric Chem. Phys.*,
907 12(19), 8963–8977, doi:10.5194/acp-12-8963-2012, 2012.
- 908 Field, P. R., Wood, R., Brown, P. R. A., Kaye, P. H., Hirst, E., Greenaway, R. and Smith, J.
909 A.: Ice Particle Interarrival Times Measured with a Fast FSSP, *J. Atmospheric Ocean.
910 Technol.*, 20(2), 249–261, doi:10.1175/1520-0426(2003)020<0249:IPITMW>2.0.CO;2, 2003.
- 911 Findeisen, W.: Kolloid-meteorologische vorgänge bei neiderschlags-bildung, *Meteorol Z.*, 55,
912 121–133, 1938.
- 913 Fridlind, A. M., Ackerman, A. S., McFarquhar, G., Zhang, G., Poellot, M. R., DeMott, P. J.,
914 Prenni, A. J. and Heymsfield, A. J.: Ice properties of single-layer stratocumulus during the
915 Mixed-Phase Arctic Cloud Experiment: 2. Model results, *J. Geophys. Res.*, 112(D24),
916 doi:10.1029/2007JD008646, 2007.
- 917 Gayet, J.-F., Crépel, O., Fournol, J.-F. and Oshchepkov, S.: A new airborne polar
918 Nephelometer for the measurements of optical and microphysical cloud properties. Part I:
919 Theoretical design, *Ann. Geophys.*, 15, 451–459, 1997.
- 920 Gayet, J.-F., Asano, S., Yamazaki, A., Uchiyama, A., Sinyul, A., Jourdan, O. and Auriol, F.:
921 Two case studies of winter continental-type water and mixed-phase stratocumuli over the sea
922 1. Microphysical and optical properties, *J. Geophys. Res.*, 107(D21),
923 doi:10.1029/2001JD001106, 2002.
- 924 Gayet, J.-F., Mioche, G., Dörnbrack, A., Ehrlich, A., Lampert, A. and Wendisch, M.:
925 Microphysical and optical properties of Arctic mixed-phase clouds. The 9 April 2007 case
926 study., *Atmospheric Chem. Phys.*, 9(17), 6581–6595, doi:10.5194/acp-9-6581-2009, 2009.
- 927 Gerber, H., Takano, Y., Garrett, T. J. and Hobbs, P. V.: Nephelometer measurements of the
928 asymmetry parameter, volume extinction coefficient and backscatter ratio in Arctic clouds, *J.
929 Atmospheric Sci.*, 57, 3021–3034, 2000.
- 930 Gultepe, I. and Isaac, G. A.: Effects of air mass origin on Arctic cloud microphysical
931 parameters for April 1998 during FIRE.ACE, *J. Geophys. Res.*, 107(C10),
932 doi:10.1029/2000JC000440, 2002.
- 933 Gultepe, I., Isaac, G., Hudak, D., Nissen, R. and Strapp, J. W.: Dynamical and Microphysical
934 Characteristics of Arctic Clouds during BASE, *J. Clim.*, 13(7), 1225–1254, doi:10.1175/1520-
935 0442(2000)013<1225:DAMCOA>2.0.CO;2, 2000.
- 936 Guyot, G., Gourbeyre, C., Febvre, G., Shcherbakov, V., Burnet, F., Dupont, J.-C., Sellegri, K.
937 and Jourdan, O.: Quantitative evaluation of seven optical sensors for cloud microphysical
938 measurements at the Puy-de-Dôme Observatory, France, *Atmospheric Meas. Tech.*, 8(10),
939 4347–4367, doi:10.5194/amt-8-4347-2015, 2015.

- 940 Herber, A., Gayet, J.-F., Hara, K., Krecji, R., Minikin, A., Neuber, R., Ritter, C., Schrems, O.,
 941 Ström, J., Schwarzenboeck, A., Treffeisen, R., Yamagata, S. and Yamanouchi, T.: Arctic
 942 Study of Tropospheric Aerosols, Clouds and Radiation, ASTAR 2004: First Results, Budapest,
 943 Hongry., 2004.
- 944 Heymsfield, A. J.: On measurements of small ice particles in clouds: SMALL PARTICLES
 945 IN ICE CLOUDS, *Geophys. Res. Lett.*, 34(23), n/a-n/a, doi:10.1029/2007GL030951, 2007.
- 946 Heymsfield, A. J., Winker, D. and Zadelhoff, G.-J.: Extinction-ice water content-effective
 947 radius algorithms for CALIPSO, *Geophys. Res. Lett.*, 32(10), doi:10.1029/2005GL022742,
 948 2005.
- 949 Hobbs, P. V., Rangno, A. L., Shupe, M. and Uttal, T.: Airborne studies of cloud structures
 950 over the Arctic Ocean and comparisons with retrievals from ship-based remote sensing
 951 measurements, *J. Geophys. Res.*, 106(D14), 15029, doi:10.1029/2000JD900323, 2001.
- 952 Hogan, R. J., Mittermaier, M. P. and Illingworth, A. J.: The Retrieval of Ice Water Content
 953 from Radar Reflectivity Factor and Temperature and Its Use in Evaluating a Mesoscale
 954 Model, *J. Appl. Meteorol. Climatol.*, 45(2), 301–317, doi:10.1175/JAM2340.1, 2006.
- 955 Jackson, R. C., McFarquhar, G. M., Korolev, A. V., Earle, M. E., Liu, P. S. K., Lawson, R. P.,
 956 Brooks, S., Wolde, M., Laskin, A. and Freer, M.: The dependence of ice microphysics on
 957 aerosol concentration in arctic mixed-phase stratus clouds during ISDAC and M-PACE, *J.*
 958 *Geophys. Res.*, 117(D15207), doi:10.1029/2012JD017668, 2012.
- 959 Jourdan, O., Mioche, G., Garrett, T. J., Schwarzenböck, A., Vidot, J., Xie, Y., Shcherbakov,
 960 V., Yang, P. and Gayet, J.-F.: Coupling of the microphysical and optical properties of an
 961 Arctic nimbostratus cloud during the ASTAR 2004 experiment: Implications for light-
 962 scattering modeling, *J. Geophys. Res.*, 115(D23206), doi:10.1029/2010JD014016, 2010.
- 963 Kay, J. E. and Gettelman, A.: Cloud influence on and response to seasonal Arctic sea ice loss,
 964 *J. Geophys. Res.*, 114(D18204), doi:10.1029/2009JD011773, 2009.
- 965 Kay, J. E., Holland, M. M., Bitz, C. M., Blanchard-Wrigglesworth, E., Gettelman, A., Conley,
 966 A. and Bailey, D.: The Influence of Local Feedbacks and Northward Heat Transport on the
 967 Equilibrium Arctic Climate Response to Increased Greenhouse Gas Forcing, *J. Clim.*, 25(16),
 968 5433–5450, doi:10.1175/JCLI-D-11-00622.1, 2012.
- 969 Klein, S. A., McCoy, R. B., Morrison, H., Ackerman, A. S., Avramov, A., Boer, G. de, Chen,
 970 M., Cole, J. N. S., Del Genio, A. D., Falk, M., Foster, M. J., Fridlind, A., Golaz, J.-C.,
 971 Hashino, T., Harrington, J. Y., Hoose, C., Khairoutdinov, M. F., Larson, V. E., Liu, X., Luo,
 972 Y., McFarquhar, G. M., Menon, S., Neggers, R. A. J., Park, S., Poellot, M. R., Schmidt, J. M.,
 973 Sednev, I., Shipway, B. J., Shupe, M. D., Spangenberg, D. A., Sud, Y. C., Turner, D. D.,
 974 Veron, D. E., Salzen, K. von, Walker, G. K., Wang, Z., Wolf, A. B., Xie, S., Xu, K.-M.,
 975 Yang, F. and Zhang, G.: Intercomparison of model simulations of mixed-phase clouds
 976 observed during the ARM Mixed-Phase Arctic Cloud Experiment. I: single-layer cloud, *Q. J.*
 977 *R. Meteorol. Soc.*, 135(641), 979–1002, doi:10.1002/qj.416, 2009.
- 978 Knollenberg, R. G.: Techniques for probing cloud microstructure, in *Clouds, Their*
 979 *Formation, Optical Properties, and Effects*, pp. 15–91, Hobbs, P. V. and Deepak, A., New-
 980 york., 1981.

- 981 Komurcu, M., Storelvmo, T., Tan, I., Lohmann, U., Yun, Y., Penner, J. E., Wang, Y., Liu, X.
 982 and Takemura, T.: INter-comparison of the cloud water phase among global climate models:
 983 cloud water phase in GCMs, *J. Geophys. Res. Atmospheres*, 119, 3372–3400,
 984 doi:10.1002/2013JD021119, 2014.
- 985 Korolev, A.: Limitations of the Wegener–Bergeron–Findeisen Mechanism in the Evolution of
 986 Mixed-Phase Clouds, *J. Atmospheric Sci.*, 64(9), 3372–3375, doi:10.1175/JAS4035.1, 2007.
- 987 Korolev, A. and Isaac, G.: Phase transformation of mixed-phase clouds, *Q. J. R. Meteorol.*
 988 *Soc.*, 129(587), 19–38, doi:10.1256/qj.01.203, 2003.
- 989 Korolev, A., Khain, A., Pinsky, M. and French, J.: Theoretical study of mixing in liquid
 990 clouds – Part 1: Classical concept, *Atmospheric Chem. Phys. Discuss.*, 15(21), 30211–30267,
 991 doi:10.5194/acpd-15-30211-2015, 2015.
- 992 Korolev, A. V., Strapp, J. W., Isaac, G. A. and Nevzorov, A. N.: The Nevzorov Airborne Hot-
 993 Wire LWC–TWC Probe: Principle of Operation and Performance Characteristics, *J.*
 994 *Atmospheric Ocean. Technol.*, 15(6), 1495–1510, doi:10.1175/1520-
 995 0426(1998)015<1495:TNAHWL>2.0.CO;2, 1998.
- 996 Korolev, A. V., Isaac, G. A. and Hallett, J.: Ice particle habits in Arctic clouds, *Geophys. Res.*
 997 *Lett.*, 26(9), 1299–1302, 1999.
- 998 Korolev, A. V., Isaac, G. A., Cober, S. G., Strapp, J. W. and Hallett, J.: Microphysical
 999 characterization of mixed-phase clouds, *Q. J. R. Meteorol. Soc.*, 129(587), 39–65,
 1000 doi:10.1256/qj.01.204, 2003.
- 1001 Korolev, A. V., Emery, E. F., Strapp, J. W., Cober, S. G., Isaac, G. A., Wasey, M. and
 1002 Marcotte, D.: Small Ice Particles in Tropospheric Clouds: Fact or Artifact? Airborne Icing
 1003 Instrumentation Evaluation Experiment, *Bull. Am. Meteorol. Soc.*, 92(8), 967–973,
 1004 doi:10.1175/2010BAMS3141.1, 2011.
- 1005 Korolev, A. V., Emery, E. F., Strapp, J. W., Cober, S. G. and Isaac, G. A.: Quantification of
 1006 the Effects of Shattering on Airborne Ice Particle Measurements, *J. Atmospheric Ocean.*
 1007 *Technol.*, 30(11), 2527–2553, doi:10.1175/JTECH-D-13-00115.1, 2013.
- 1008 Lampert, A., Ehrlich, A., Dörnbrack, A., Jourdan, O., Gayet, J.-F., Mioche, G., Shcherbakov,
 1009 V., Ritter, C. and Wendisch, M.: Microphysical and radiative characterization of a subvisible
 1010 midlevel Arctic ice cloud by airborne observations – a case study, *Atmospheric Chem. Phys.*,
 1011 9(8), 2647–2661, doi:10.5194/acp-9-2647-2009, 2009.
- 1012 Lance, S., Shupe, M. D., Feingold, G., Brock, C. A., Cozic, J., Holloway, J. S., Moore, R. H.,
 1013 Nenes, A., Schwarz, J. P., Spackman, J. R., Froyd, K. D., Murphy, D. M., Brioude, J.,
 1014 Cooper, O. R., Stohl, A. and Burkhardt, J. F.: Cloud condensation nuclei as a modulator of ice
 1015 processes in Arctic mixed-phase clouds, *Atmospheric Chem. Phys.*, 11(15), 8003–8015,
 1016 doi:10.5194/acp-11-8003-2011, 2011.
- 1017 Law, K. S., Ancellet, G., Pelon, J., Turquety, S., Clerbaux, C., Pommier, M., de Villiers, R.,
 1018 Gayet, J.-F., Schwarzenboeck, A., Nedelec, P., Schneider, J. and Borrmann, S.: POLARCAT-
 1019 France Airborne Experiment: first results, pp. 7–12, Annecy, France., 2008.

- 1020 Lawson, R. P. and Baker, B. A.: Improvement in Determination of Ice Water Content from
 1021 Two-Dimensional Particle Imagery. Part II: Applications to Collected Data, *J. Appl.*
 1022 *Meteorol. Climatol.*, 45(9), 1291–1303, doi:10.1175/JAM2399.1, 2006.
- 1023 Lawson, R. P., Baker, B. A., Schmitt, C. G. and Jensen, T. L.: An overview of microphysical
 1024 properties of Arctic clouds observed in May and July 1998 during FIRE ACE, *J. Geophys.*
 1025 *Res.*, 106(D14), 14989, doi:10.1029/2000JD900789, 2001.
- 1026 Lefèvre, R.: Physique de la mesure de la sonde CPI pour la mesure des propriétés des cristaux
 1027 de glace. Application aux observations réalisées durant la campagne ASTAR 2004.,
 1028 Université Blaise Pascal, Aubière, France., 2007.
- 1029 Libbrecht, K. G.: The physics of snow crystals, *Rep. Prog. Phys.*, 68(4), 855–895,
 1030 doi:10.1088/0034-4885/68/4/R03, 2005.
- 1031 Liu, Y., Key, J. R., Ackerman, S. A., Mace, G. G. and Zhang, Q.: Arctic cloud macrophysical
 1032 characteristics from CloudSat and CALIPSO, *Remote Sens. Environ.*, 124, 159–173,
 1033 doi:10.1016/j.rse.2012.05.006, 2012.
- 1034 Lloyd, G., Choularton, T. W., Bower, K. N., Crosier, J., Jones, H., Dorsey, J. R., Gallagher,
 1035 M. W., Connolly, P., Kirchgaessner, A. C. R. and Lachlan-Cope, T.: Observations and
 1036 comparisons of cloud microphysical properties in spring and summertime Arctic
 1037 stratocumulus clouds during the ACCACIA campaign, *Atmospheric Chem. Phys.*, 15(7),
 1038 3719–3737, doi:10.5194/acp-15-3719-2015, 2015.
- 1039 McFarquhar, G. M., Zhang, G., Poellot, M. R., Kok, G. L., McCoy, R., Tooman, T., Fridlind,
 1040 A. and Heymsfield, A. J.: Ice properties of single-layer stratocumulus during the Mixed-Phase
 1041 Arctic Cloud Experiment: 1. Observations, *J. Geophys. Res.*, 112(D24201),
 1042 doi:10.1029/2007JD008633, 2007.
- 1043 McFarquhar, G. M., Ghan, S., Verlinde, J., Korolev, A., Strapp, J. W., Schmid, B.,
 1044 Tomlinson, J. M., Wolde, M., Brooks, S. D., Cziczo, D., Dubey, M. K., Fan, J., Flynn, C.,
 1045 Gultepe, I., Hubbe, J., Gilles, M. K., Laskin, A., Lawson, P., Leaitch, W. R., Liu, P., Liu, X.,
 1046 Lubin, D., Mazzoleni, C., Macdonald, A.-M., Moffet, R. C., Morrison, H., Ovchinnikov, M.,
 1047 Shupe, M. D., Turner, D. D., Xie, S., Zelenyuk, A., Bae, K., Freer, M. and Glen, A.: Indirect
 1048 and Semi-direct Aerosol Campaign: The Impact of Arctic Aerosols on Clouds, *Bull. Am.*
 1049 *Meteorol. Soc.*, 92(2), 183–201, doi:10.1175/2010BAMS2935.1, 2011.
- 1050 Meyers, M. P., DeMott, P. J. and Cotton, W. R.: New Primary Ice-Nucleation
 1051 Parameterizations in an Explicit Cloud Model, *J. Appl. Meteorol.*, 31(7), 708–721,
 1052 doi:10.1175/1520-0450(1992)031<0708:NPINPI>2.0.CO;2, 1992.
- 1053 Mioche, G.: Validation des produits d'inversion des observations satellitaires CALIPSO et
 1054 CloudSat pour la caractérisation des propriétés optiques et microphysiques des nuages de
 1055 glace et en phase mixte, Université Blaise Pascal, Aubière, France., 2010.
- 1056 Mioche, G., Jourdan, O., Ceccaldi, M. and Delanoë, J.: Variability of mixed-phase clouds in
 1057 the Arctic with a focus on the Svalbard region: a study based on spaceborne active remote
 1058 sensing, *Atmospheric Chem. Phys.*, 15(5), 2445–2461, doi:10.5194/acp-15-2445-2015, 2015.

- 1059 Morrison, H. and Pinto, J. O.: Intercomparison of Bulk Cloud Microphysics Schemes in
 1060 Mesoscale Simulations of Springtime Arctic Mixed-Phase Stratiform Clouds, *Mon. Weather*
 1061 *Rev.*, 134(7), 1880–1900, doi:10.1175/MWR3154.1, 2006.
- 1062 Morrison, H., de Boer, G., Feingold, G., Harrington, J., Shupe, M. D. and Sulia, K.:
 1063 Resilience of persistent Arctic mixed-phase clouds, *Nat. Geosci.*, 5(1), 11–17,
 1064 doi:10.1038/ngeo1332, 2012.
- 1065 Nakaya, U.: *Snow Crystals: Natural and Artificial*, Cambridge Harvard University Press.,
 1066 1954.
- 1067 Ovchinnikov, M., Ackerman, A. S., Avramov, A., Cheng, A., Fan, J., Fridlind, A. M., Ghan,
 1068 S., Harrington, J., Hoose, C., Korolev, A., McFarquhar, G. M., Morrison, H., Paukert, M.,
 1069 Savre, J., Shipway, B. J., Shupe, M. D., Solomon, A. and Sulia, K.: Intercomparison of large-
 1070 eddy simulations of Arctic mixed-phase clouds: Importance of ice size distribution
 1071 assumptions, *J. Adv. Model. Earth Syst.*, 6(1), 223–248, doi:10.1002/2013MS000282, 2014.
- 1072 Pinto, J. O.: Autumnal Mixed-Phase Cloudy Boundary Layers in the Arctic, *J. Atmospheric*
 1073 *Sci.*, 55(11), 2016–2038, doi:10.1175/1520-0469(1998)055<2016:AMPCBL>2.0.CO;2, 1998.
- 1074 Pinto, J. O. and Curry, J. A.: Cloud-aerosol interactions during autumn over Beaufort Sea, *J.*
 1075 *Geophys. Res.*, 106(D14), 15077–15097, 2001.
- 1076 Prenni, A. J., DeMott, P. J., Kreidenweis, S. M., Harrington, J. Y., Avramov, A., Verlinde, J.,
 1077 Tjernström, M., Long, C. N. and Olsson, P. Q.: Can Ice-Nucleating Aerosols Affect Arctic
 1078 Seasonal Climate?, *Bull. Am. Meteorol. Soc.*, 88(4), 541–550, doi:10.1175/BAMS-88-4-541,
 1079 2007.
- 1080 Prenni, A. J., Demott, P. J., Rogers, D. C., Kreidenweis, S. M., Mcfarquhar, G. M., Zhang, G.
 1081 and Poellot, M. R.: Ice nuclei characteristics from M-PACE and their relation to ice formation
 1082 in clouds, *Tellus B*, 61(2), 436–448, doi:10.1111/j.1600-0889.2009.00415.x, 2009.
- 1083 Protat, A., Delanoë, J., Bouniol, D., Heymsfield, A. J., Bansemer, A. and Brown, P.:
 1084 Evaluation of Ice Water Content Retrievals from Cloud Radar Reflectivity and Temperature
 1085 Using a Large Airborne In Situ Microphysical Database, *J. Appl. Meteorol. Climatol.*, 46(5),
 1086 557–572, doi:10.1175/JAM2488.1, 2007.
- 1087 Protat, A., Delanoë, J., Strapp, J. W., Fontaine, E., Leroy, D., Schwarzenboeck, A., Lilie, L.,
 1088 Davison, C., Dezitter, F., Grandin, A. and Weber, M.: The Measured Relationship between
 1089 Ice Water Content and Cloud Radar Reflectivity in Tropical Convective Clouds, *J. Appl.*
 1090 *Meteorol. Climatol.*, 55(8), 1707–1729, doi:10.1175/JAMC-D-15-0248.1, 2016.
- 1091 Pruppacher, H. R. and Klett, J. D.: *Microphysics of Clouds and Precipitation*, Springer
 1092 Netherlands, Dordrecht. [online] Available from: [http://link.springer.com/10.1007/978-94-](http://link.springer.com/10.1007/978-94-009-9905-3)
 1093 [009-9905-3](http://link.springer.com/10.1007/978-94-009-9905-3) (Accessed 22 December 2015), 1978.
- 1094 Quennehen, B., Schwarzenboeck, A., Schmale, J., Schneider, J., Sodemann, H., Stohl, A.,
 1095 Ancellet, G., Crumeyrolle, S. and Law, K. S.: Physical and chemical properties of pollution
 1096 aerosol particles transported from North America to Greenland as measured during the
 1097 POLARCAT summer campaign, *Atmospheric Chem. Phys.*, 11(21), 10947–10963,
 1098 doi:10.5194/acp-11-10947-2011, 2011.

- 1099 Rangno, A. L. and Hobbs, P. V.: Ice particles in stratiform clouds in the Arctic and possible
 1100 mechanisms for the production of high ice concentrations, *J. Geophys. Res.*, 106(D14),
 1101 15065, doi:10.1029/2000JD900286, 2001.
- 1102 Savre, J. and Ekman, A. M. L.: Large-eddy simulation of three mixed-phase cloud events
 1103 during ISDAC: Conditions for persistent heterogeneous ice formation: LES OF ICE
 1104 NUCLEATION DURING ISDAC, *J. Geophys. Res. Atmospheres*, 120(15), 7699–7725,
 1105 doi:10.1002/2014JD023006, 2015.
- 1106 Schwarzenboeck, A., Mioche, G., Armetta, A., Herber, A. and Gayet, J.-F.: Response of the
 1107 Nevzorov hot wire probe in clouds dominated by droplet conditions in the drizzle size range,
 1108 *Atmospheric Meas. Tech.*, 2(2), 779–788, doi:10.5194/amt-2-779-2009, 2009.
- 1109 Shupe, M. D. and Intrieri, J. M.: Cloud Radiative Forcing of the Arctic Surface: The Influence
 1110 of Cloud Properties, Surface Albedo, and Solar Zenith Angle, *J. Clim.*, 17(3), 616–628,
 1111 doi:10.1175/1520-0442(2004)017<0616:CRFOTA>2.0.CO;2, 2004.
- 1112 Shupe, M. D., Matrosov, S. Y. and Uttal, T.: Arctic Mixed-Phase Cloud Properties Derived
 1113 from Surface-Based Sensors at SHEBA, *J. Atmospheric Sci.*, 63(2), 697–711,
 1114 doi:10.1175/JAS3659.1, 2006.
- 1115 Shupe, M. D., Daniel, J. S., de Boer, G., Eloranta, E. W., Kollias, P., Luke, E. P., Long, C. N.,
 1116 Turner, D. D. and Verlinde, J.: A Focus On Mixed-Phase Clouds: The Status of Ground-
 1117 Based Observational Methods, *Bull. Am. Meteorol. Soc.*, 89(10), 1549–1562,
 1118 doi:10.1175/2008BAMS2378.1, 2008.
- 1119 Shupe, M. D., Walden, V. P., Eloranta, E., Uttal, T., Campbell, J. R., Starkweather, S. M. and
 1120 Shiobara, M.: Clouds at Arctic Atmospheric Observatories. Part I: Occurrence and
 1121 Macrophysical Properties, *J. Appl. Meteorol. Climatol.*, 50(3), 626–644,
 1122 doi:10.1175/2010JAMC2467.1, 2011.
- 1123 Solomon, A., Feingold, G. and Shupe, M. D.: The role of ice nuclei recycling in the
 1124 maintenance of cloud ice in Arctic mixed-phase stratocumulus, *Atmospheric Chem. Phys.*,
 1125 15(18), 10631–10643, doi:10.5194/acp-15-10631-2015, 2015.
- 1126 Solomon, S., Qin, D., Manning, M., Chen, Z., Marquis, M., Averyt, K. B., Tignor, M. and
 1127 Miller, H. L.: *Climate change 2007: the physical science basis*, Cambridge University Press,
 1128 Cambridge, UK., 2007.
- 1129 Stephens, G. L., Vane, D. G., Boain, R. J., Mace, G. G., Sassen, K., Wang, Z., Illingworth, A.
 1130 J., O'Connor, E. J., Rossow, W. B., Durden, S. L., Miller, S. D., Austin, R. T., Benedetti, A.,
 1131 Mitrescu, C. and CloudSat Science Team, T.: The CloudSat mission and the A-Train: a new
 1132 dimension of space-based observations of clouds and precipitation, *Bull. Am. Meteorol. Soc.*,
 1133 83(12), 1771–1790, doi:10.1175/BAMS-83-12-1771, 2002.
- 1134 Tan, I. and Storelvmo, T.: Sensitivity Study on the Influence of Cloud Microphysical
 1135 Parameters on Mixed-Phase Cloud Thermodynamic Phase Partitioning in CAM5, *J.*
 1136 *Atmospheric Sci.*, 73(2), 709–728, doi:10.1175/JAS-D-15-0152.1, 2016.
- 1137 Ulanowski, Z., Kaye, P. H., Hirst, E., Greenaway, R. S., Cotton, R. J., Hesse, E. and Collier,
 1138 C. T.: Incidence of rough and irregular atmospheric ice particles from Small Ice Detector 3

- 1139 measurements, *Atmospheric Chem. Phys.*, 14(3), 1649–1662, doi:10.5194/acp-14-1649-2014,
1140 2014.
- 1141 Verlinde, J., Harrington, J. Y., Yannuzzi, V. T., Avramov, A., Greenberg, S., Richardson, S.
1142 J., Bahrmann, C. P., McFarquhar, G. M., Zhang, G., Johnson, N., Poellot, M. R., Mather, J.
1143 H., Turner, D. D., Eloranta, E. W., Tobin, D. C., Holz, R., Zak, B. D., Ivey, M. D., Prenni, A.
1144 J., DeMott, P. J., Daniel, J. S., Kok, G. L., Sassen, K., Spangenberg, D., Minnis, P., Tooman,
1145 T. P., Shupe, M., Heymsfield, A. J. and Schofield, R.: The Mixed-Phase Arctic Cloud
1146 Experiment, *Bull. Am. Meteorol. Soc.*, 88(2), 205–221, doi:10.1175/BAMS-88-2-205, 2007.
- 1147 Vochezer, P., Järvinen, E., Wagner, R., Kupiszewski, P., Leisner, T. and Schnaiter, M.: In situ
1148 characterization of mixed phase clouds using the Small Ice Detector and the Particle Phase
1149 Discriminator, *Atmospheric Meas. Tech.*, 9(1), 159–177, doi:10.5194/amt-9-159-2016, 2016.
- 1150 Waliser, D. E., Li, J.-L. F., Woods, C. P., Austin, R. T., Bacmeister, J., Chern, J., Del Genio,
1151 A., Jiang, J. H., Kuang, Z., Meng, H., Minnis, P., Platnick, S., Rossow, W. B., Stephens, G.
1152 L., Sun-Mack, S., Tao, W.-K., Tompkins, A. M., Vane, D. G., Walker, C. and Wu, D.: Cloud
1153 ice: A climate model challenge with signs and expectations of progress, *J. Geophys. Res.*,
1154 114, doi:10.1029/2008JD010015, 2009.
- 1155 Wegener, A.: *Thermodynamik der Atmosphäre*, J. A. Barth., Leipzig., 1911.
- 1156 Winker, D. M., Pelon, J. R. and McCormick, M. P.: The CALIPSO mission: spaceborne lidar
1157 for observation of aerosols and clouds, vol. 4893, pp. 1–11, *Proceedings of SPIE*, 4893,
1158 Hangzhou, China., 2003.
- 1159 Young, G., Connolly, P. J., Jones, H. M. and Choulaton, T. W.: Microphysical sensitivity of
1160 coupled springtime Arctic stratocumulus to modelled primary ice over the ice pack, marginal
1161 ice, and ocean, *Atmospheric Chem. Phys.*, 17(6), 4209–4227, doi:10.5194/acp-17-4209-2017,
1162 2017.
- 1163
1164

1165 **Table 1: Summary of *in situ* observations of Arctic single layer MPCs.**
 1166

Field experiment	Location [latitude range]	Date	Number of flights in MPCs	Number of profiles in MPCs	Duration of data (minutes)
ASTAR 2004	Spitzbergen (Norway) [76-79]° N	May 2004	4	7	30
ASTAR 2007	Spitzbergen (Norway) [76-79]° N	April 2007	5	34	173
POLARCAT 2008	Kiruna (Sweden) [68-73]° N	April 2008	4	10	45
SORPIC 2010	Spitzbergen (Norway) [75-78]° N	May 010	5	20	109
TOTAL			18	71	357

1167
 1168

1169 **Table 2: Uncertainties of cloud properties derived from CPI, FSSP, PN and Nevzorov instruments.**
 1170

Probe [Measurements range]	Number concentration (N)	Extinction coefficient (σ)	Effective diameter (D_{eff})	Water contents (IWC or LWC)	Asymmetry parameter (g)
CPI [15 μm to 2.3 mm]	50 %	55 %	80 %	60 %	-
FSSP-100 [3 to 45 μm]	10 %	35 %	4 %	20 %	-
PN [< 800 μm]	-	25 %	-	-	4 %
Nevzorov [LWC > 0.003-0.005 $\text{g}\cdot\text{m}^{-3}$]	-	-	-	20%	-

1171
 1172

1173
1174
1175
1176

Table 3: Statistics of cloud base and cloud top altitudes along with cloud layer thickness obtained from the 71 profiles sampled in MPCs.

	Mean	Standard dev.	Median	25th percentile	75th percentile	Max.	Min.
z_{top} (m)	1200	310	1200	1000	1370	2120	525
z_{base} (m)	756	283	700	510	850	1700	400
Layer thickness (m)	444	211	420	270	600	950	100

1177
1178

1179
 1180
 1181
 1182

Table 4: Summary of the method for the assessment of the cloud thermodynamical phase and liquid droplet and ice crystal properties from the combination of PN, CPI, FSSP and Nevzorov probes.

Instrument [measurement range]	PN g-values [corresponding cloud phase]		
	$g < 0,80$ [ice]	$0,80 < g < 0,83$ [mixed]	$g > 0,83$ [liquid]
FSSP [15 to 45 μm]	NO	YES	YES
Nevzorov probe [LWC > 0.003-0.005 g.m-3]	NO	YES	YES
CPI [15 μm to 2.3 mm]	YES	YES	NO

1183
 1184

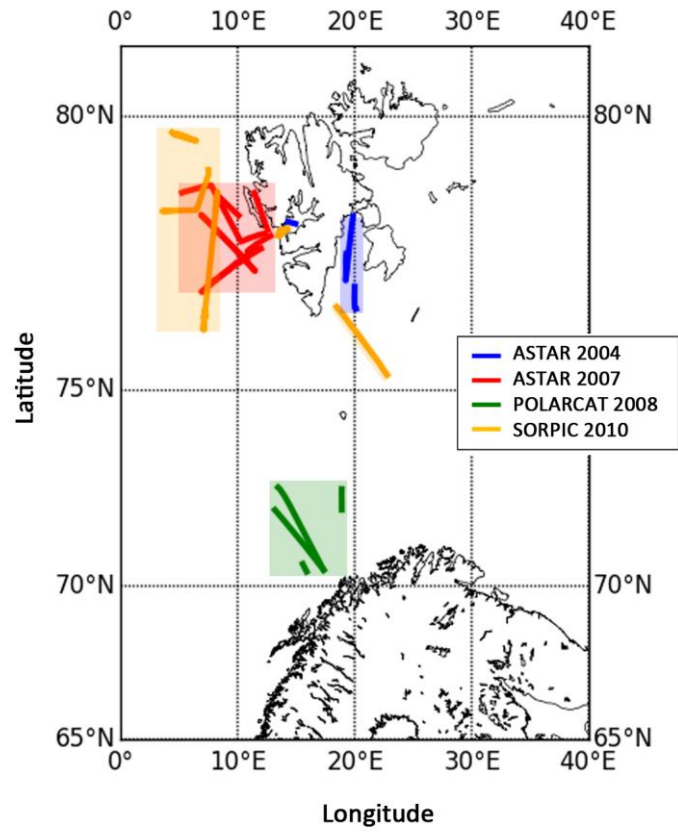
1185
1186
1187

Table 5: Classification of the MPC situations according to temperature regimes and air mass origins

Experiment	Date	Mean T_{Top} (°C)	Air mass origin N = North (Arctic Ocean) S/E = South or East (Continental)	Regime
ASTAR 2004	15 may	-16,5	N	COLD
	22 may	-8,5	S	WARM_SO
	25 may	-8	N	WARM_NO
	5 june	-11	N	WARM_NO
ASTAR 2007	2 april	-21	N	COLD
	3 april	-16	N	COLD
	7 april	-22	N	COLD
	8 april	-19	N	COLD
	9 april	-21	N	COLD
POLARCAT 2008	31 march	-15	N	WARM_NO
	1 st april	-10	N	WARM_NO
	10 april	-14	N	WARM_NO
	11 april	-14	N	WARM_NO
SORPIC 2010	4 may	-13	SE	WARM_SO
	5 may	-11	SE	WARM_SO
	6 may	-13	SE	WARM_SO
	9 may	-15	S	WARM_SO
	10 may	-13,5	N	WARM_NO

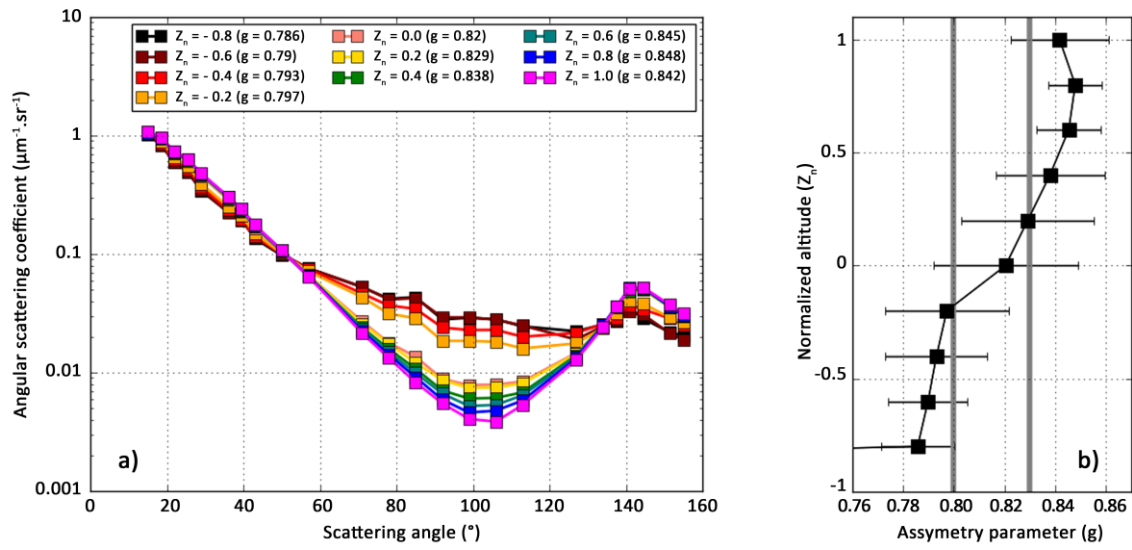
1188

1189
1190



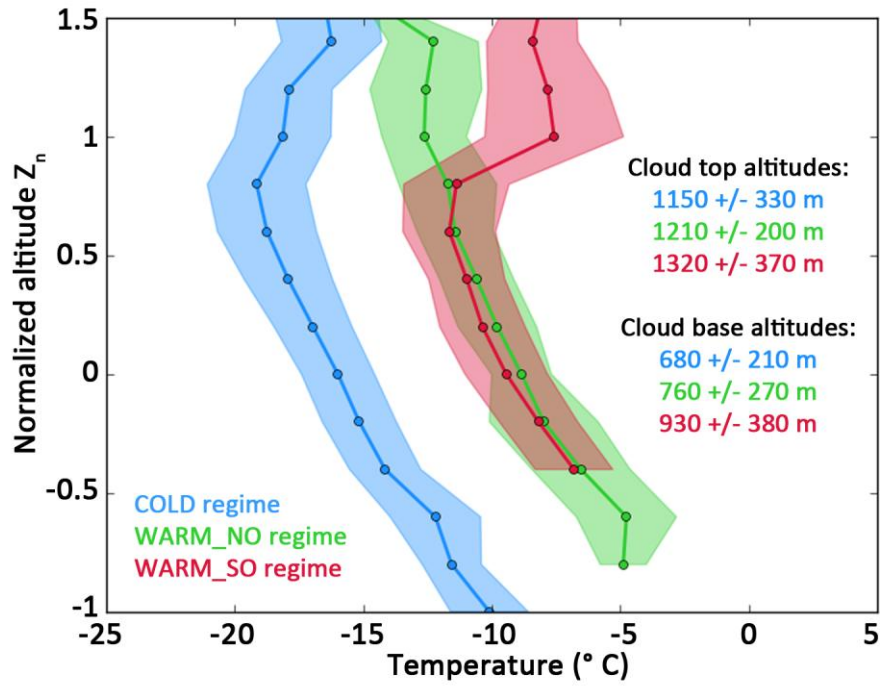
1191
1192
1193
1194

Figure 1: Location of the MPC measurements during the ASTAR, POLARCAT and SORPIC campaigns.



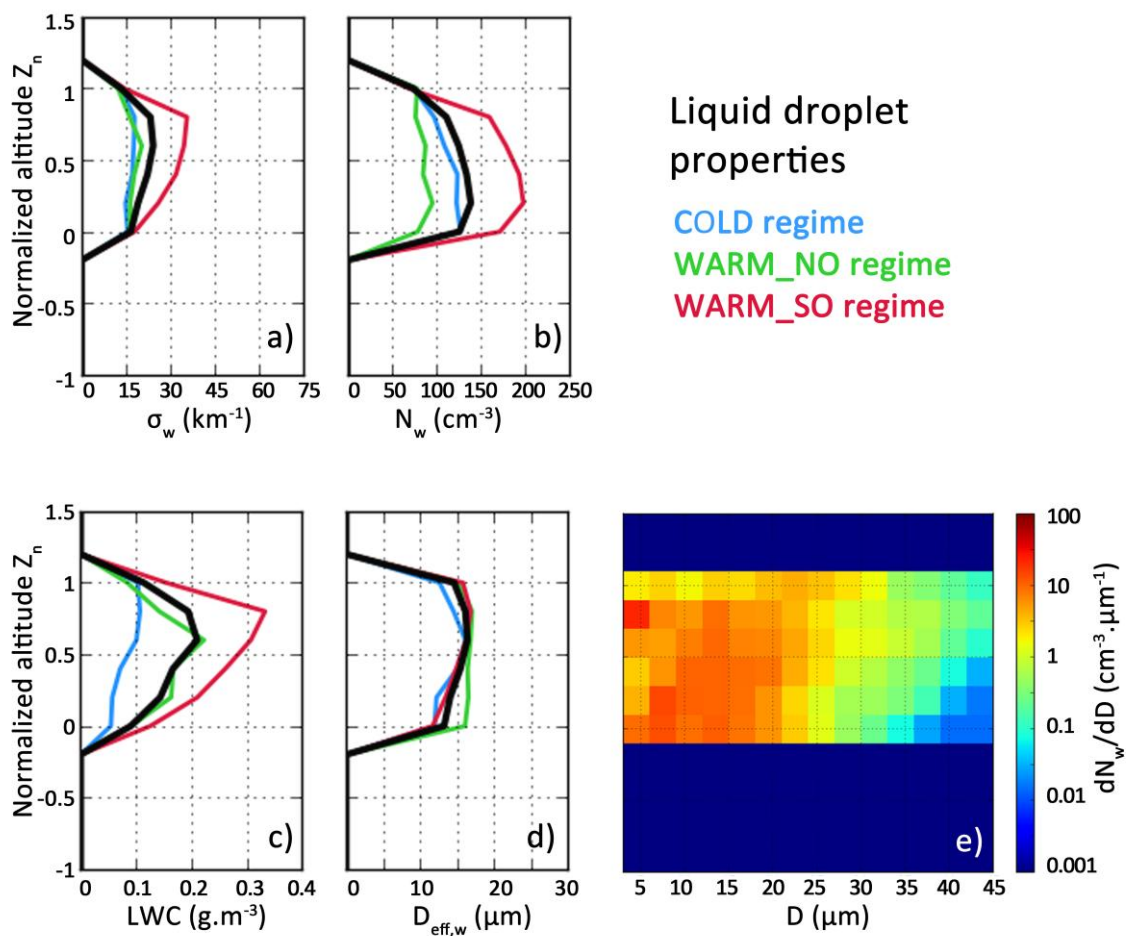
1195
1196

1197 **Figure 2: a): Normalized scattering phase function according to the normalized altitude from Polar Nephelometer**
 1198 **measurements (few μm to around $800 \mu\text{m}$ size range), averaged over all the campaigns. g -values indicate the cloud**
 1199 **phase: $g < 0.80$: ice, $0.80 < g < 0.83$: mixed and $g > 0.83$: liquid. b): Mean vertical profile of asymmetry parameter (for**
 1200 **all the campaigns). The grey bars indicate the threshold g -values for the assessment of ice, mixed and liquid cloud**
 1201 **phases.**
 1202



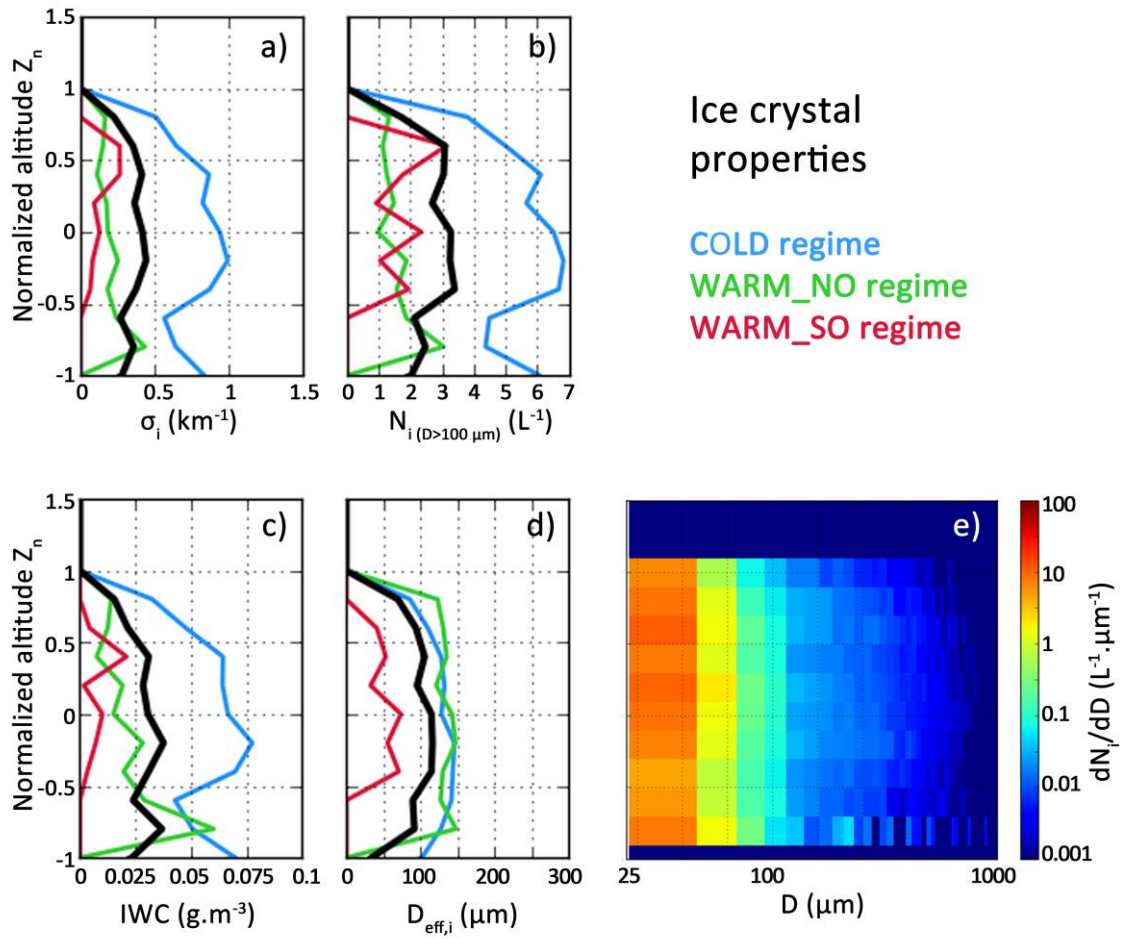
1203
 1204
 1205
 1206
 1207
 1208
 1209

Figure 3: Vertical profiles (normalized altitude) of the mean temperature for each regime. Shaded spreads represent the standard deviation. The mean cloud base and top altitudes and their standard deviation for each regime are indicated.



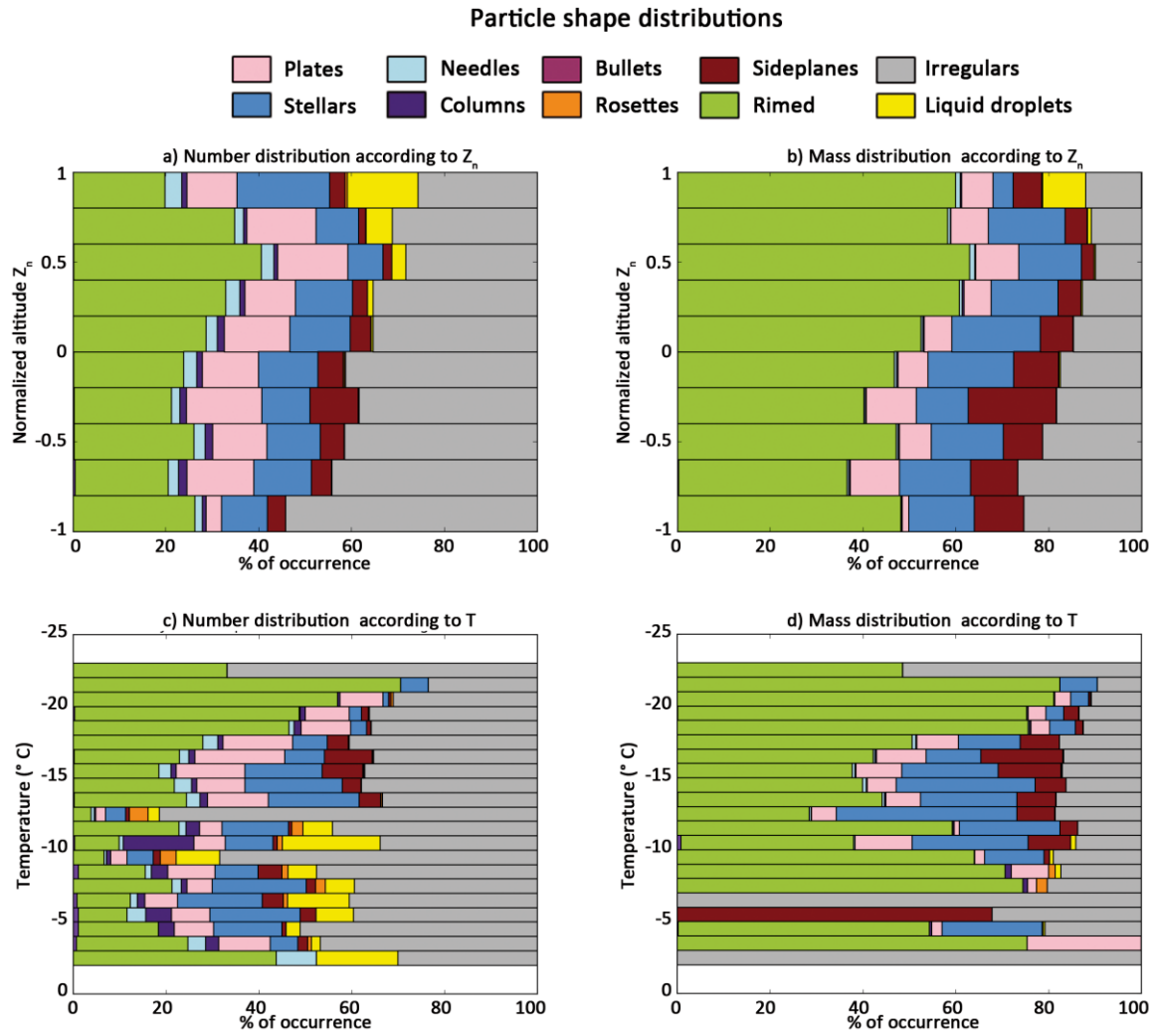
1210
 1211
 1212
 1213
 1214
 1215
 1216
 1217
 1218

Figure 4: Vertical profiles (expressed in normalized altitude) of liquid droplets properties from FSSP or Nevzorov probe measurements (3-45 μm size range): a) extinction coefficient, b) droplet concentration, c) LWC, d) effective diameter for the three regimes and averaged over all the campaigns and e) averaged droplet size distribution for all the campaigns.



1219
 1220
 1221
 1222
 1223
 1224

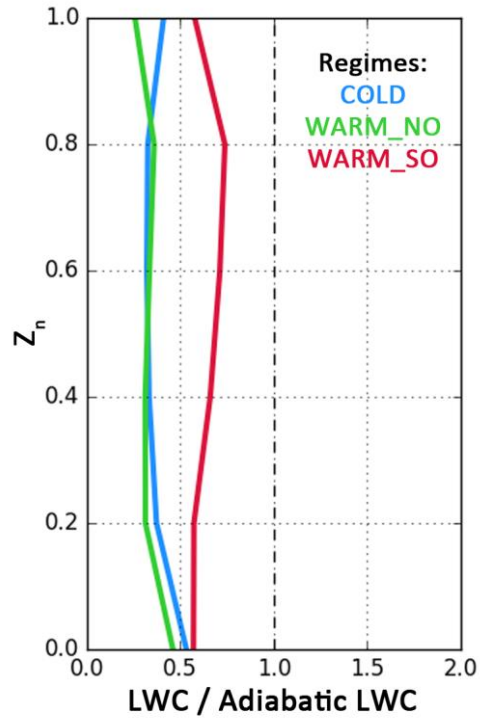
Figure 5: Vertical profiles (expressed in normalized altitudes) of ice crystal properties from CPI measurements (15 μm - 2.3 mm size range): a) extinction coefficient, b) ice crystal concentration, c) IWC, d) effective diameter for the three regimes and averaged over all the campaigns and e) averaged particle size distribution for all the campaigns.



1225
 1226
 1227
 1228
 1229
 1230
 1231

Figure 6: Vertical profiles of particle shapes (from CPI measurements and for particles larger than 100 μm) according to normalized altitude (top panels) and temperature (bottom panels). Distributions are displayed according to particle number (left panels) and mass (right panels).

1232



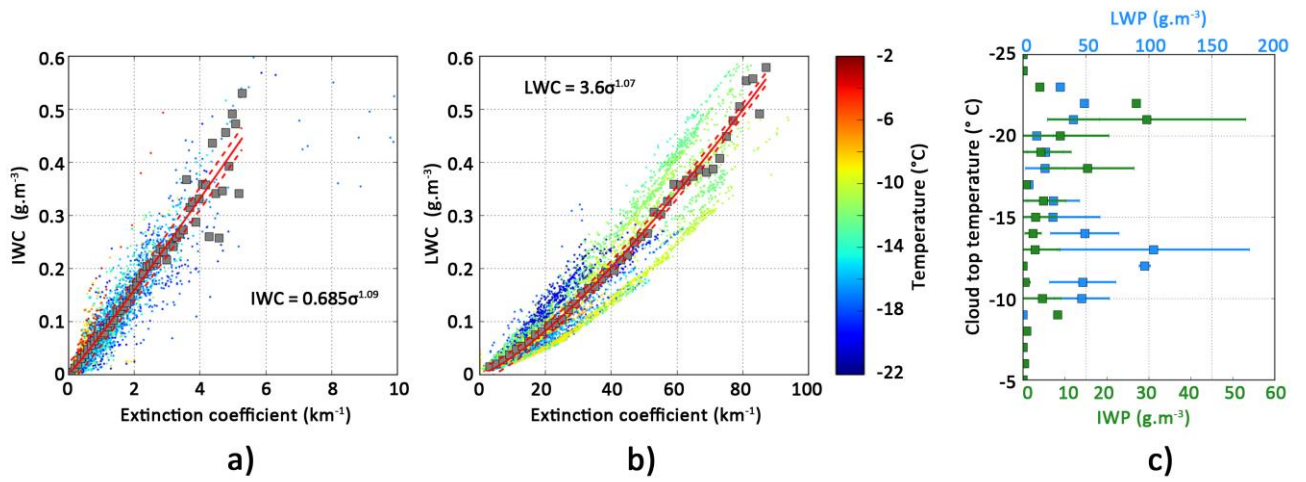
1233

1234

1235

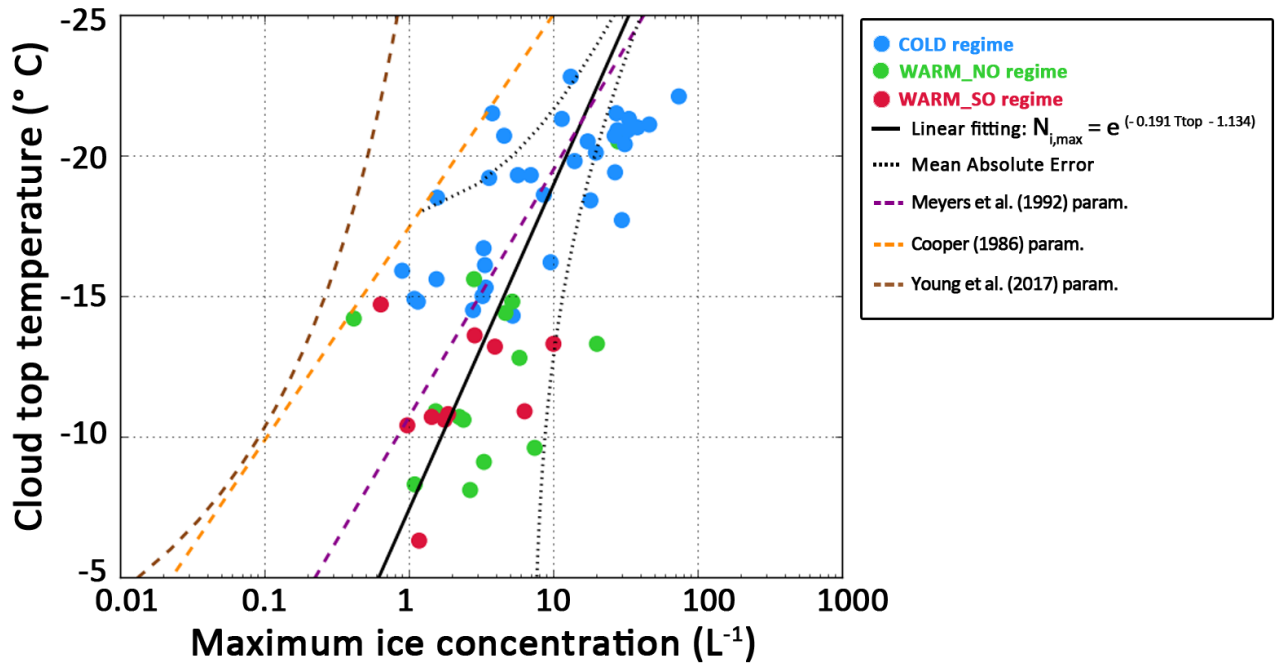
Figure 7: Vertical profiles of the ratio of measured LWC over theoretical adiabatic LWC for the three regimes.

1236



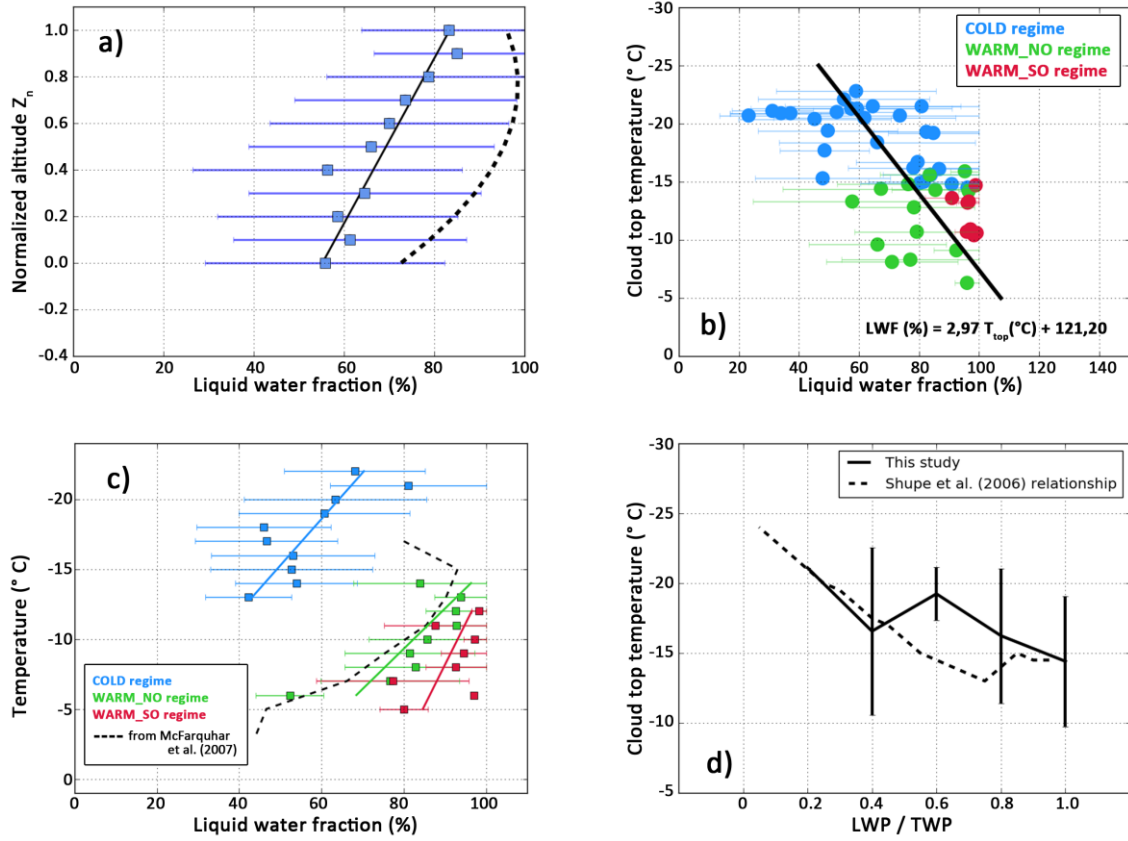
1237
 1238
 1239
 1240
 1241
 1242
 1243
 1244

Figure 8: a) IWC and b) LWC as a function of extinction coefficient. Color scale is the temperature, grey squares represent the values averaged over extinction coefficient intervals of 0.1 km^{-1} and 2 km^{-1} for IWC and LWC respectively. The red lines represent the curve fittings and the dashed-line the uncertainties on the fitted relationships (Mean Absolute Errors). c) Ice (green) and liquid (blue) water paths according to the cloud top temperature.



1245
 1246
 1247
 1248
 1249
 1250
 1251

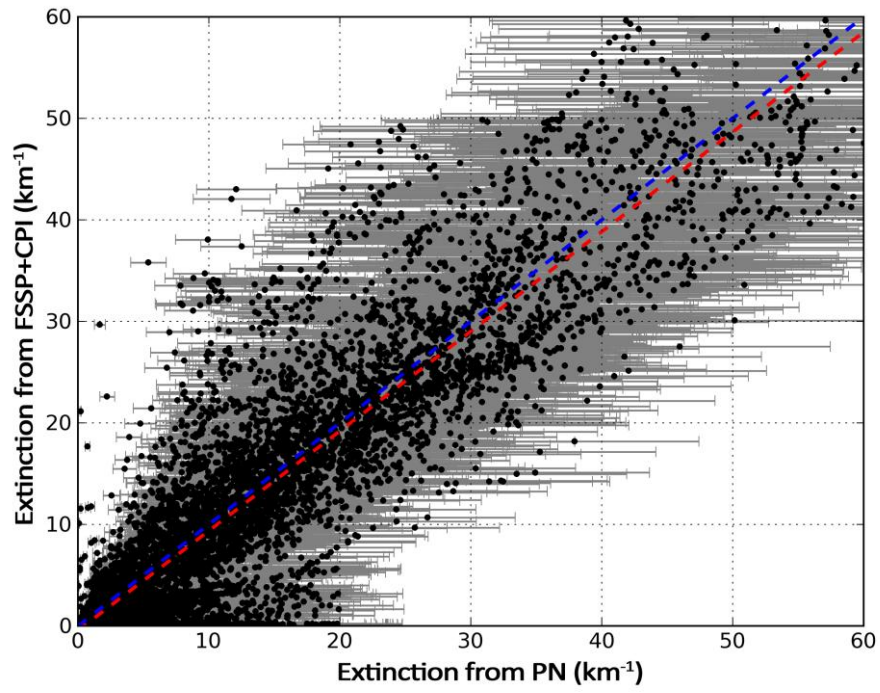
Figure 9: Maximum ice crystal concentration as a function of cloud top temperature. The colored circles represent the values for each profile (with fitting in black solid line and mean absolute error in dotted lines). The Meyers et al. (1992), Cooper (1986) and Young et al. (2017) parameterizations are also displayed in purple, orange and brown dashed lines respectively.



1252
 1253
 1254
 1255
 1256
 1257
 1258

Figure 10: Liquid water fraction according to Z_n (a), cloud top temperature (b) and temperature (c). The dotted dashed line on panels a) and c) is the parameterization from McFarquhar et al. (2007) and the solid lines on panels a), b) and c) are the fittings for the present study. d) Ratio of LWP over TWP according to cloud top temperature. The solid line refers to the present study and the dotted lines refers to Shupe et al. (2006) work.

1259



1260

1261

1262 **Figure B1: Comparison of extinction from PN and CPI+FSSP measurements. Grey bars represent the 25 %**

1263 **uncertainties on the PN extinction. The red dotted line is the linear fitting (slope of 0.98, R² = 0.87) and the blue dotted**

1264 **line is the 1:1 line.**